INDONESIAN JOURNAL ON GEOSCIENCE
Geological Agency
Ministry of Energy and Mineral Resources

Journal homepage: http://ijog.geologi.esdm.go.id
ISSN 2355-9314, e-ISSN 2355-9306

Secondary Enrichment of REE in Weathered Granite, South Bangka, Indonesia

Armin Tampubolon[1,2], Ildrem Syafri[1], Mega Fatimah Rosana[1], and Euis Tintin Yuningsih[1]

[1]Faculty of Geological Engineering, Padjadjaran University, Bandung, West Java, Indonesia
[2] Research Center for Geological Resources, National Research and Innovation Agency

Corresponding author: armin.tampubolon@gmail.com/ildrem@unpad.ac.id/mega85unpad@gmail.com/e.tintin@unpad.ac.id
Manuscript received: June, 23, 2023; revised: October, 25, 2023;
approved: January, 15, 2024; available online: April, 17, 2024

Abstract – Rare earth elements (REEs) are essential materials for the manufacture of advanced technology. Secondary REE indications were found in alluvial and lateritic tin deposits within Southeast Asia Tin Belt. This study aims at the REE enrichment of weathering profiles underlain by Toboali Pluton of the main range S-type granite of this belt. Granite and weathering samples were collected and analyzed using XRF, ICP-MS/OES, XRD, SEM-EDX, and EPMA. The Chondrite-normalized REE patterns of granite in Toboali showed enrichment in REE with the highest value of 1,126 ppm. The Toboali Pluton is enriched in LREE and depleted in HREE. The enrichment of REE from the upper to lower horizon of weathering profiles was pointed out by the increase in REE values from a range of 156-188 ppm (horizon B) to 196-268 ppm (horizon C) in Toboali, and from a range of 230-330 ppm (horizon B) to 342-450 ppm (horizon C) in Air Gegas. These coincided with the presence of kaolinite with elevated REE and CeO_2 in horizon C of weathering profile. Leaching test result proved that kaolinite plays a role in REE enrichment in the weathering profile through ion adsorption mechanisms in the Air Gegas. The weathering process of REE fluoro-carbonate (bastnäsite-(Ce)) and parisite-(Ce) in granite is believed to contribute in enrichment due to its high dissolution rate, which enhances kaolinite adsorption. In contrast, REE phosphates such as monazite-(Ce) and xenotime-(Y), because of their strong resistance and low solubility, are thought to be only slightly soluble, and most of these minerals remain in Toboali weathering products.

Keywords: weathering profiles, horizon C, kaolinite, REE fluoro-carbonate, REE phosphate

How to cite this article:
Tampubolon, A., Syafri, I., Rosana, M.F., and Yuningsih, E.T., 2024. Secondary Enrichment of REE in Weathered Granite, South Bangka, Indonesia. *Indonesian Journal on Geoscience*, 11 (1), p.141-165. DOI: 10.17014/ijog.11.1.141-165

Introduction

Background

Rare earth elements (REE) consist of seventeen elements from the lanthanide group (La, Ce, Pr, Nd, Pm, Sm, Eu, Gd, Tb, Dy, Ho, Er, Tm, Yb, and Lu), including Y and Sc which have similar chemical properties (Yang *et al*., 2019). REE is essential for the manufacture of advanced technology such as computers, cellular phones, TVs, laser beams, missile weapons, electric vehicles, and environmentally-friendly future energy raw materials (Phillip, 2017; Weng *et al*., 2017). They are categorized as critical raw materials based on the level of supply risk (George *et al*., 2015). China dominates the world in terms of resources, production, and supply of REE commodities (Dickson, 2015).

In Indonesia, REE studies primarily focused on utilizing minerals as by-products of tin alluvial. According to regional metallogeny, such by-products are part of the Southeast Asia Tin Belt, where

REEs have been identified in Thailand, Laos, and Malaysia (Imai, 2009; Sanematsu *et al*., 2009). Secondary REEs were found in an alluvial tin or lateritic weathering deposits such as monazite-(Ce), zircon, and xenotime-(Y) in South Bangka (Hamdan and Rusmana, 2003). The enrichment in laterite originated from granite within Southeast Asia Tin Belt, occuring in Lingga Island of Riau Islands in the northwest with REE grade is fourfold compared to underlain granite (Irzon *et al*., 2016). REE in the weathering profile originates from the underlying bedrock during the weathering process. REEs are transported downward from the uppermost part, and redistributed into minerals or adsorbed on weathering products when lower-pH soil water comes in contact with higher-pH groundwater (Sanematsu *et al*., 2013). The REEs complexes and REE^{3+} are positively charged and adsorbed onto negatively charged clay minerals (Feng *et al*., 2021). Substitution of surface Si^{4+} or Al^{3+} by cations of lower valency leads to negative charges on the surface of kaolinite, facilitating REEs binding by electrostatic attraction (Coppin *et al*., 2002; Moldoveanu and Papangelakis, 2016). The REE accumulates in weathering profile as a result of both mass transfer and eluviation-illuviation mechanisms (Li *et al*., 2017).

Occurrences of ion-adsorption-type prospects outside China were identified in Laos and northern Vietnam, north of the Southeast Asia Tin Belt. These occurrences are enhanced by the tropical climate in Southeast Asia, which promotes the weathering of granites in southern China (Sanematsu *et al*., 2009). Similar to China and Laos, Indonesia has a comparable climate and lithological structure. This condition would lead to REE most likely being mobilized and fractionated during intense weathering of the granite (Xu *et al*., 2017). Indonesian granites identified as biotite granite have REE content of 298 ppm in Toboali, 302-316 ppm in Pading, and 274 ppm in Permisan (Ng *et al*., 2017). The occurrence of REE in weathering crusts of such granitic rocks has not yet been investigated although weathering products such as laterite and alluvium have large areas within South Bangka (Hamdan, 2004).

The studied areas situated in South Bangka Regency, Bangka-Belitung Province, are parts of REE inventory project areas of the Directorate General of Mineral and Coal, Ministry of Energy and Mineral Resources of Indonesia. The area can be reached from Pangkal Pinang, the provincial city of Bangka-Belitung, through a good asphaltic road for 1.5 hours by vehicle to Toboali. The aim of this paper is to reveal REE enrichment in the weathering process on granite. It also discusses REE value patterns in the weathered horizons of underlain granite and the potentially REE-bearing mineral as REEs sources. The role of kaolinite in the secondary enrichment of REE in the weathering profiles is described.

Geological Settings

Bangka Island, as the southern part of the Southeast Asian Tin Belt, is occupied by Triasic-Jurasic I-type and S-type Klabat granite intruding the Carboniferous to Permian Pemali Complex and Triassic Tanjung Genting Formation. The former, Pemali Complex, is composed of phyllites, schists, and gneisses, whilst the latter comprises intercalating siltstone, sandstone, claystone, and metasediments (Margono *et al*., 1995). Klabat Granite which consists of granite, granodiorite, adamelite, diorite, and quartz diorites is well distributed in the western, southern, central, and eastern parts of Bangka, with ages ranging from Late Permian to Late Triassic periods (Kurnia and Priadi, 2013; Ng *et al*., 2017).

Granites in Bangka Island are subdivided into metaluminous and peraluminous monzogranites classified as high K- and shoshonite types within syn-collisional and mantle tectonics (Shita and Lucas, 2009). Granites in the eastern and central Bangka originated from the crust-mantle mixing environment with its magma affinity of calc-alkaline type, specifically I-type. Furthermore, in southern and western Bangka, they originated from a crust with high magma affinity of K-calc-alkaline S-type (Kurnia and Priadi, 2013). The granitic rocks of central and eastern Bangka exhibit more primitive character as they have varieties of magnetite and magnesium minerals, while the southern

and western Bangka ones have been identified as S-type granite due to high K_2O in addition to abundant alumina minerals such as biotite, muscovite, and cordierite (Kurnia and Priadi, 2013).

Previous studies identified granitic rocks in southern Bangka as biotite and hornblende biotite granites (Ng *et al*., 2017). Such granite covers the southeastern, middle, and western parts of South Bangka (Figure 1). Referring to chondrite-normalized LREE patterns, Toboali granite was classified as I-type. However, based on the Zr/Y ratio, the negative anomaly of Eu indicates an affinity for a high-K calc-alkaline suite. These features characterize the S-type granite character that originated from continental magma (Aryanto and Kamiludin, 2016). The two information about the types of granite affinities mentioned above are contradictory, but in reality, they tend to be types of I and IS as compiled in Figure 1.

Age dating was performed in previous studies, specifically for tin-bearing Klabat monzogranites 211 ± 10-200 ±4 Ma or Upper Triassic, respectively (Marker, 2013). Such rocks were formed from magma and occurred due to greywacke material located within the collision horizon of the continental rim. Granite of Toboali and Simpang Rimba, South Bangka, are aged 217 ± 15 and 213 ± 4 Ma (Schwartz *et al*., 1995). Other studies reported that granite outcrop in South Bangka has similarities with Malaysia's Main Range (Ng *et al*., 2017). The granite was derived from two magmatic episodes in which the older plutonic granite was emplaced in the northeast at 225 Ma, while the younger pluton occurred in the southwest at 220 Ma (Ng *et al*., 2017).

Methods and Materials

Methods

Granitic rock samples were taken by chip sampling using a hammer of approximately 2 kg. Meanwhile, samples from the weathered profile were collected by channel sampling using a small shovel vertically from top to bottom along the same horizon. Cumulative weathering samples were quartered to reduce for approximately 2 kg.

Petrographic descriptions of granitoid samples were carried out at the laboratory of the Centre for Mineral Coal and Geothermal Resources, Geo-

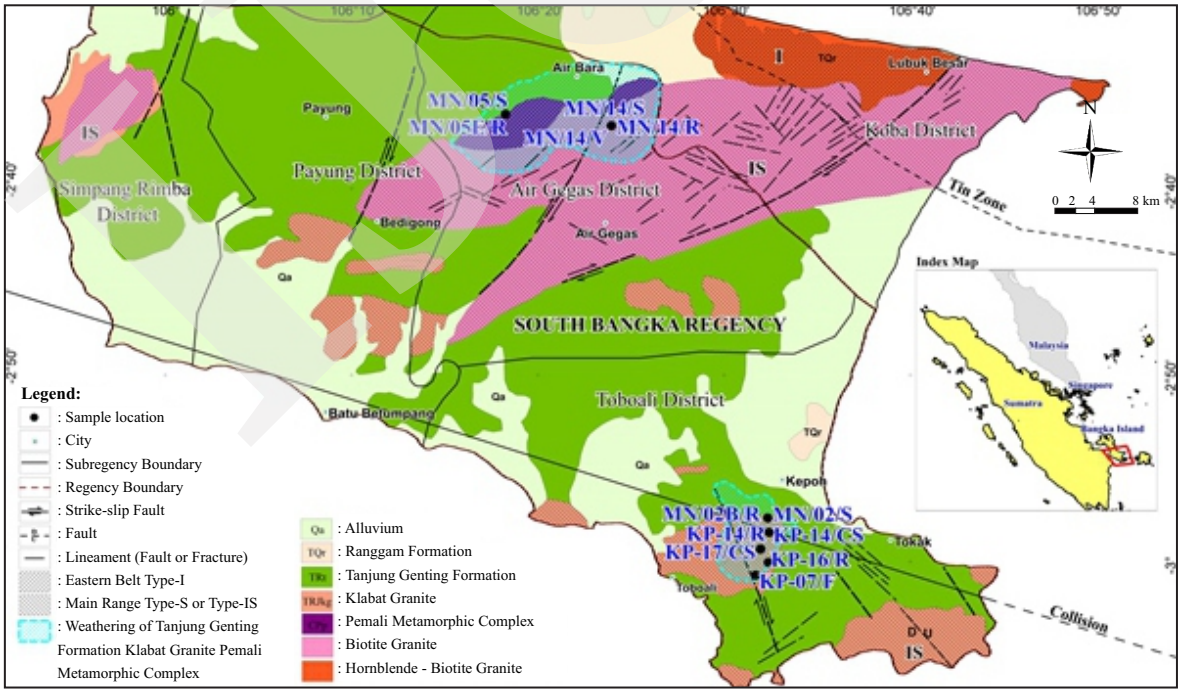

Figure 1. Geological map of the studied area (modified from Crow and Van Leeuwen, 2005; Aryanto and Kamiludin, 2016; Ng *et al*., 2017) and sample localities.

logical Agency of Indonesia. X-Ray Fluorescence analyzer (XRF) was conducted to determine major elements using PANalytical B.V- MagiX FAST XRF at Intertek Laboratory Jakarta, Indonesia. Inductively Coupled Plasma Mass Spectrometry (ICP-MS) was performed to analyze the REE using ICP-MS Agilent type 7700. While Inductively Coupled Plasma Optical Emission Spectrometry (ICP-OES) analyses were conducted to determine trace elements using ICP-OES Agilent type 725. These ICP-MS and ICP-OES analysis were performed at Intertek Laboratory Jakarta, Indonesia. Samples were dried, crushed by a jaw crusher or iron mortar, and ground by a mill. The solution of rock samples for ICP-MS analyses was made by acid digestion of fused glass beads using lithium metaborate and tetraborate as flux.

X-Ray Diffraction (XRD) was performed at the laboratory of the Centre for Geological Survey, Geological Agency of Indonesia, and Laboratory Wuhan Centre, China Geological Survey (CGS). Rock or solid samples for laboratory analysis were prepared to have bulk powder by the agate grinding to the required grain size of about 200 mesh. Weathering materials (soil and clay) samples were dried in an oven at 50-60ºC before being ground to 200 mesh, then placed on a flat sample holder and leveled.

The main XRD instrument used is PANalytical X'Pert PRO with type series of PW3040/x0 X'Pert PRO, made in Netherland. For the test of sample materials totally, they used Cu-tube with a spinning sample holder or flat sample holder. The measurement angle (2-theta) used to perform was around 3-60°. The grinding tools used were agate grinders with grain sizes ranging from 5-10 um or approximately 200 mesh. The determination of bulk compositions applied in The Wuhan Centre is based on the method described by Chung (1974). Whereas samples detected at the laboratory of The Centre for Geological Survey are interpreted using the software X'Pert HighScore with X'Pert Data Viewer.

Scanning Electron Microscope-Energy Dispersive Spectroscopy (SEM-EDS) applied for analysis was of type JEOL JED-2200 Series (SEM JEOL-JSM6360LA) performed at the Wuhan Centre, CGS, China Laboratory. Some selected samples were analyzed using Electron Probe Microanalyzer (EPMA) and Backscattered Electron (BSE). The chemical compositions of minerals were measured using a Shimadzu Electron Probe Microanalyzer (EPMA 1600). At the same time, BSE images were also taken. The operating conditions were set during quantitative analysis: 15 kV accelerating voltage, 10 nA beam current, and 1 μm beam diameter. Minerals from the SPI Company of America were used as standards, and a programme based on the ZAF procedure was used for data correction.

A leaching test was carried out on the premise that this process is a reversible reaction, as evidence that cations and negatively charged surfaces are mechanisms for REE adsorption (Alshameri *et al*., 2019). REE adsorbed on clay can easily be removed with monovalent salt solutions such as ammonium sulfate, because it is easier to exchange REE ions (Zhang *et al*., 2017). The leaching test was performed at The Laboratory of Mineral and Coal Test of The Directorate General of Mineral and Coal, Ministry of Energy and Mineral Resources of Indonesia in Bandung. Preparation was carried out by grinding 5 gr of weathering samples using an agate grinder to a size of 200 mesh. Ground samples were weighed 3 or 5 gr, and then mixed with 10 ml of ammonium sulfate solution with 1 M concentration at pH 5 and 9 so that the REE recovery, especially La, would increase sharply at that concentration (Feng *et al*., 2021). Afterward, it is stirred using a magnetic stirrer for 1 hour at a speed of 250 rpm and a temperature of 28° C. The stirring results are filtered through a fine sieve coated with filter paper discs and vacuumed to separate leachate and residue. The residue was placed in the oven for 18 hours at 101° C and analyzed afterward using ICP-OES.

Weathering Profile

Five of weathering profiles were the focus of observations and are depicted in Figure 1; three in Toboali, and two in Air Gegas (Figure 2). The

location of the MN/02/S Toboali weathering profile is in an abandoned tin mine pit, with a laterite horizon thickness of 6 m (Figure 2a). The topsoil was removed during the mining operation. Samples from the upper horizon (0-3 m) or B is light brown laterite, with dominant clay-sand-grained size, pebble, and poorly compacted. The lower horizon (3-6 m) or C is reddish brown, with dominant sand-grained size, pebble, and poorly compacted. A big boulder of slightly weathered granite, suspected as the base of the lateritic profile, shows a medium-grained size.

The KP17/CS Toboali weathering profile is in a tin pit mine, underlain by alluvial deposits, consisting of four horizons (Figure 2b), and close to granite outcrops of sample KP/16/R. Topsoil or horizon A (0-0.7m) is dark brown, loose, composed of organic matter, roots, and hummus. Horizon B (0.7-1.7m) shows grey and poorly compacted, comprises clay minerals and slightly fine sand. Horizon C (1.7-5.5m) is yellowish-white and somewhat compressed. Horizon D (5.5-6.7m) is light whitish grey, comprises quartzite gravel, minor sand, and clay minerals. The base of the weathering profile is slightly compacted

Weathering profile of KP/14/CS, Toboali consists of horizons A, B, C, and D (Figure 2c). Horizon A (0.-0.2m) is composed of topsoil showing dark brown, porous, and organic matter (hummus). Horizon B (0.2-2.7m) shows light reddish-brown, completely weathered, and poorly compacted. Horizon C (2.7-3.2m) shows yellowish brown, composed of sub-weathered/saprolite, quartz, and felsic mineral relics. Horizon D (3.2-4.2m) shows slightly weathered granitoid, yellowish brown-greyish black, composed of quartz, feldspar, biotite, and clay minerals.

Weathering profile of sample MN/05/S in Air Gegas (Figure 2d) located at a tin mining pit consisting of horizon B and C. Horizon B as the upper horizon (0-4m) shows yellowish red, and comprises of soil, quartz, clay minerals, minor rock fragments, and incompact. While the lower horizon C (4-8m) has reddish-brown, subweathered, poorly compacted, and consists of quartz, clays, and visible relics of feldspar and biotite. The base of the mining pit observed is parts of a quartz vein mixed with granite-forming minerals; it is cream and composed of cloudy quartz and weathered feldspar. This profile inferred to

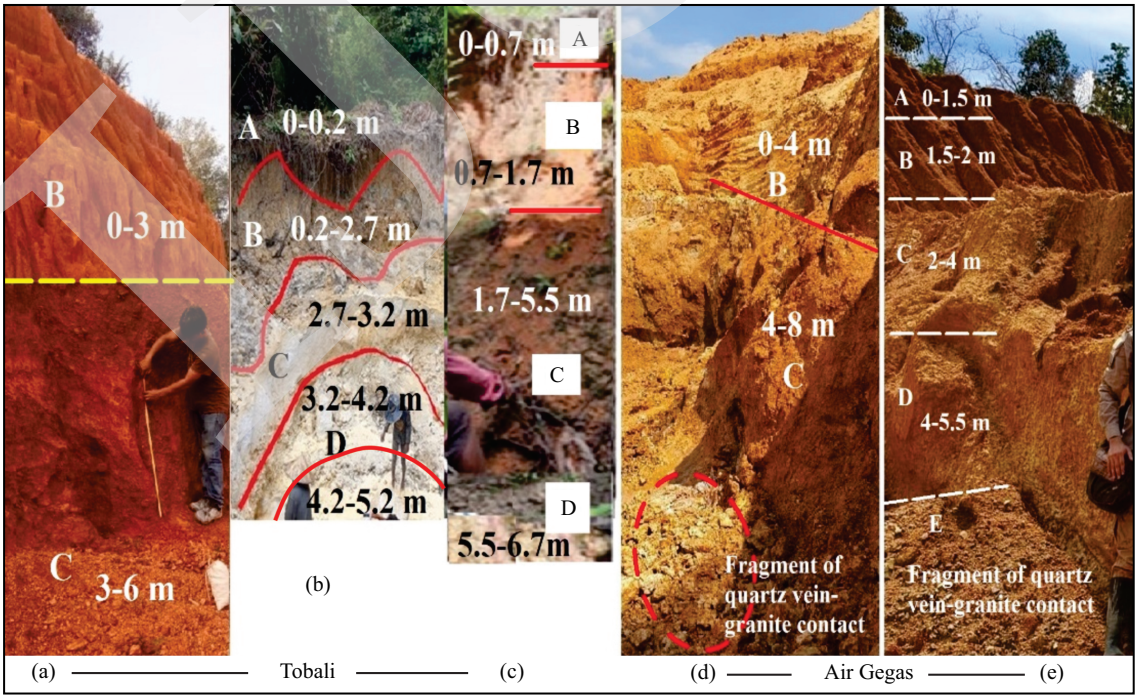

Figure 2. Field photographs showing weathering profile of (a) MN/02/S; (b) KP/17/CS; (c) and KP/14/CS in Toboali; (d) MN/05/S; and (e) MN/14/S in Air Gegas.

result from the weathering process of underlain biotite granite, referring to lithological units of the published geological map (Mangga and Djamal, 1994).

Weathering profile at the sample location of MN/14/S, Air Gegas (Figure 2e) comprises horizons A, B, C, D, and E (Figure 2e). Horizon A (0-1.5m) is the topsoil which is dark brown, loose, porous, and composed of quartz minerals, organic matter, roots, sand, and clay. Horizon B (1.5-2m) shows fully weathered, reddish grey, and poorly compacted, and is composed of quartz, limonite, clay minerals, and sand. Horizon C (2-4m) is completely weathered, light brown, poorly compacted, and composed of quartz, clay minerals, and sand. Horizon D (4-5.5 m) is brown, subweathered granite with feldspar and quartz relics. Basement (E) is composed of quartz vein-tourmaline in granite (MN/14/R), and broken quartz vein-granite contact (MN/14/V).

Granite

A research on Toboali Pluton in this area was carried out recently in the REE inventory project, and several samples were selected to observe. Four of these are of concern, because they are close to the weathering profile. The four samples namely MN/02B/R, KP/14/R, KP/16/R, and KP/07/F are located on the Toboali Pluton (Ng *et.al*., 2017). In general, this pluton has a medium texture. It consists mainly of quartz, orthoclase, plagioclase, hornblende, and biotite. While two granite samples, MN/05E/R and MN/14/R in Air Gegas contain mineralized quartz veins as the base of the weathering profile. Fragments of rock-forming minerals, such as quartz and orthoclase, are mixed with hydrothermal quartz veins.

The granite sample MN/02B/R is thought to be the source of REE in horizons MN/02/S (0-3 m) and (3-6 m) which form an overlying weathering profile (Figure 2a). Sample MN/02B/R was identified as syenogranite and the other two (KP/14/R and KP/16/R) as granite. Such samples are part of Toboali Plutons (Ng *et al*., 2017), recognized to form in younger magmatic episodes, which are found on the southwestern side of Bangka. These plutons have an average magmatic age of ca. 220 Ma (Ng *et al*., 2017).

Granite harboring quartz veins were found at the base of weathering profile in the tin mine pit of Air Gegas (MN/5E/R). No fresh granite was observed at the bottom of the tin pits, because groundwater seepage inundated this zone (Figure 2d).

Result

Petrographic Description

The petrographic description on a granite sample of MN/02B/R underlying weathering profile from Toboali shows colourless, holocrystalline, hypidiomorphic granular, fine to 8.0 mm grain size, euhedral to anhedral crystals (Figure 3). Using a comparison chart (Terry and Chilingar, 1955), the composition of the rock-forming minerals were estimated. It is composed of quartz (35 %), orthoclase (30 %), plagioclase (5 %), microcline (12 %), hornblende (6 %), biotite (4 %), clay (3 %), monazite (1 %), zircon (1 %), chlorite (1 %) and opaque minerals (2 %). The plot of the composition of this sample on the Streckeisen diagram denotes syenogranite.

The granite sample KP/14/R under microscopic observation comprises quartz (60 %), orthoclase (26 %), muscovite (5 %), chlorite (3 %), plagioclase (4 %), opaque minerals (2 %) (Figure 3a and b). While granite sample KP/16/R is composed of quartz (66 %), orthoclase (15 %), plagioclase (5 %), clay (5 %), hornblende (3 %), muscovite (2 %), chlorite (2 %), epidote (1 %), and opaque minerals (1 %) (Figure 4c and d).

The petrographic description of the MN/05E/R sample indicated the presence of rock-forming minerals such as orthoclase and quartz, along with monazite and zircon (Figure 5a and b). Likewise, MN/14/R, part of the quartz veins in granite, has subhedral to anhedral crystal forms consisting of quartz, pyroxene, and cassiterite (Figure 5c and d). Based on the plot of composition data on the Streckeisen diagram, samples are classified as alkali-feldspar granite

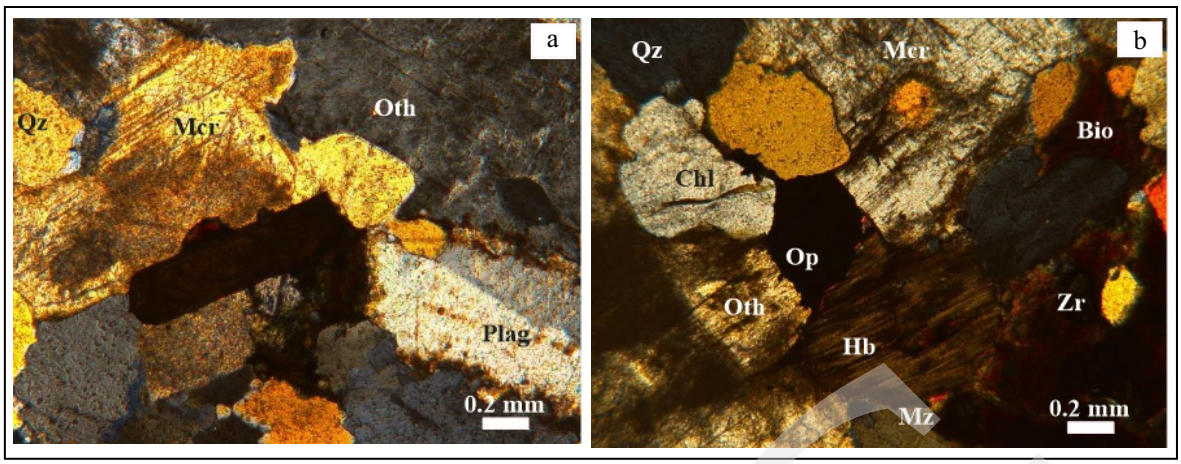

Figure 3. Photomicrographs of thin section sample TBL-21MN/02B/R, Toboali. a). Cross Nicol, showing microcline (Mcr) with irregular brownish-yellow crystal, plagioclase (Plag) with prismatic twin crystal, orthoclase (Oth) with pale grey, and quartz (Qz) with yellow anhedral crystal. b). Cross Nicol, showing quartz (Qz), microcline (Mcr), orthoclase (Oth), biotite (Bio), hornblende (Hb) with dark greenish- brown, chlorite (Chl) with blackish-white, zircon (Zr) with yellow sub-euhedral crystal, monazite (Mz) with bright pinkish-yellow, and opaque minerals with black euhedral crystal.

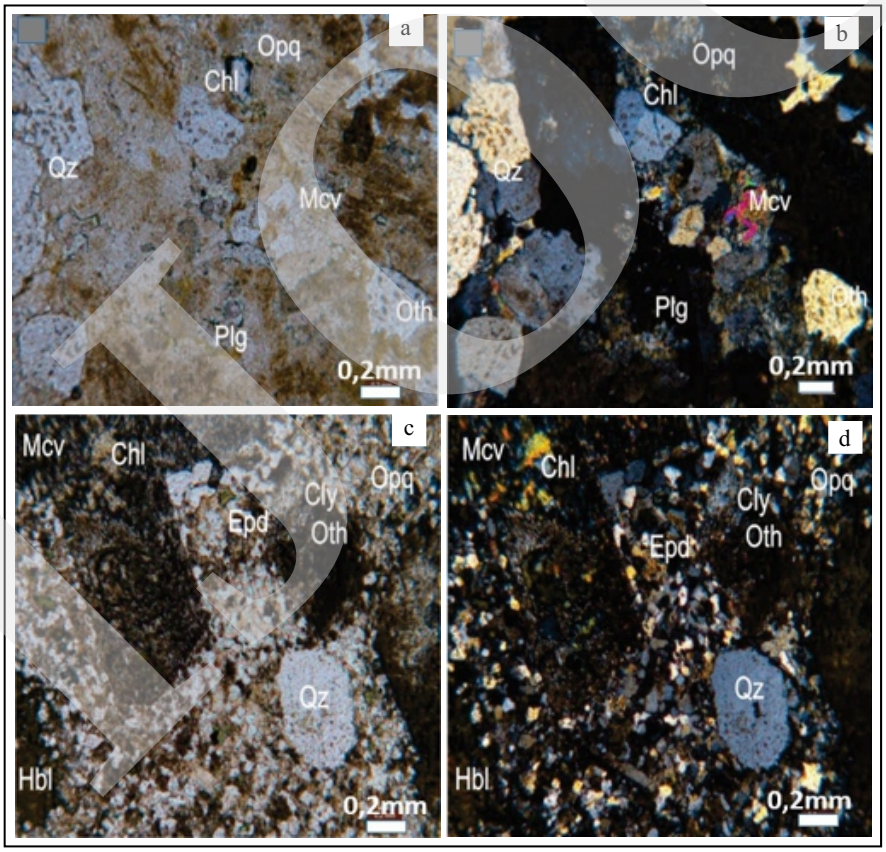

Figure 4. Photomicrographs of granite sample KP/14/R (a) under parallel nicol; (b) cross nicol. Photomicrographs of granite sample KP/16/R (c) under parallel nicol; and (d) cross nicol. Qz = quartz, Oth = orthoclase, Plg = plagioclase, Mcv = muscovite, Hbl = hornblende, Bt = biotite, Epd = epidote, Cly = clay, Opq = opaque minerals, Chl = chlorite.

and quartz-rich granitoid (Figure 6). Plotting data of major elements from the previous analysis results (Table 1) onto a diagram of Batchelor and Bowden's (1985), the researched area is classified tectonically in the syn-collision zone (Figure 6b).

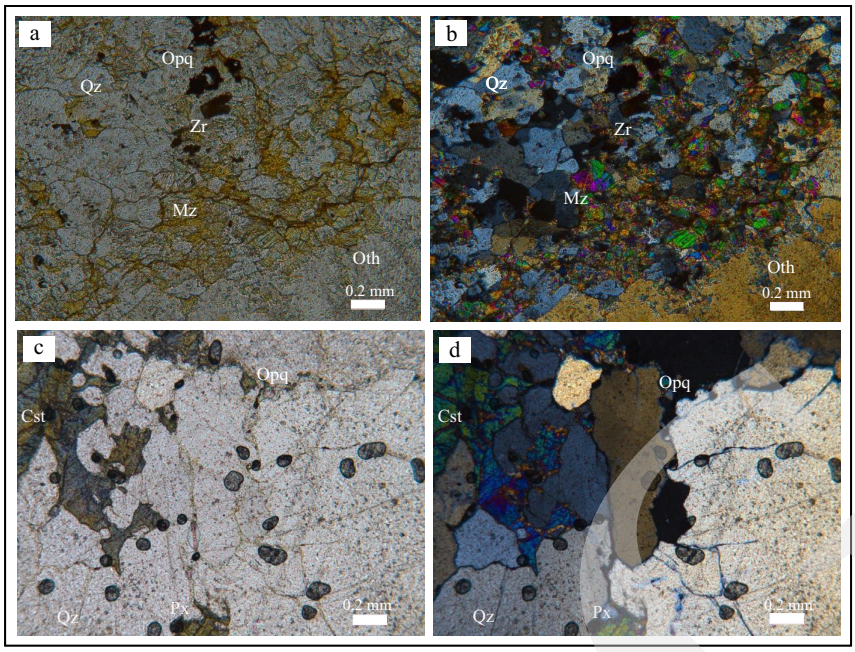

Figure 5. Photomicrographs of sample MN/5E/R, Air Gegas: (a) under parallel nicol and (b) crossed nicol; composed mainly of quartz veins (Qz), orthoclase (Oth), monazite (Mz), zircon (Zr) and opaque minerals (Opq). The contact between quartz veins (Qz) and granitoid (b) is shown. Photomicrographs of sample MN/14/R, Air Gegas, (c) under parallel nicol; and (d) crossed nicol; composed of quartz (93%), cassiterite (Cst) (5 %), pyroxene (Px) (1 %), and opaque minerals (1 %). It is part of quartz veins in contact with granitoids.

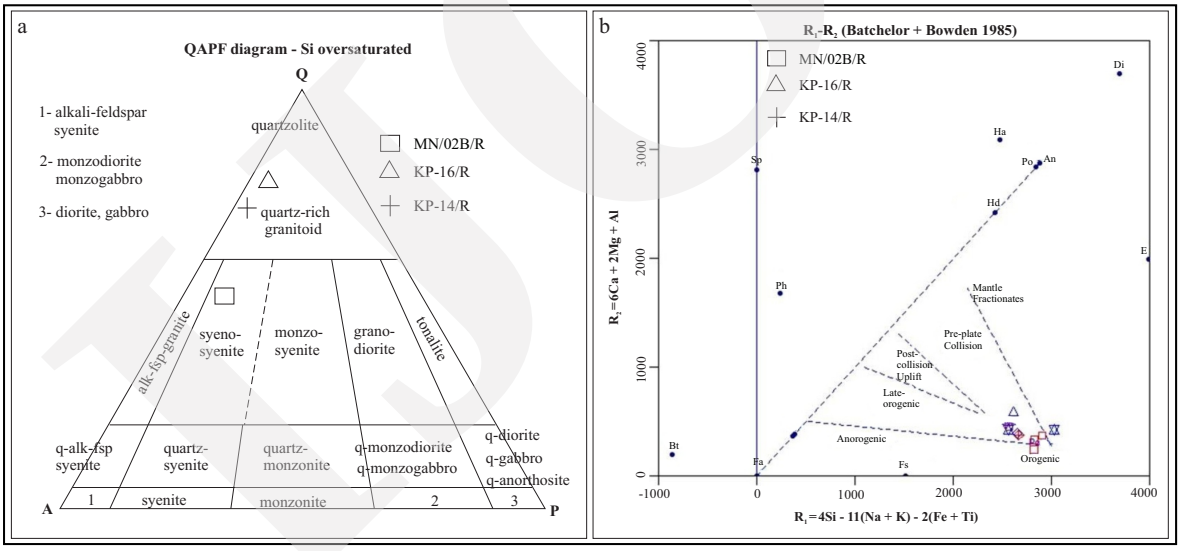

Figure 6. a). Plot of granitic rock composition on QAPF diagram (Streckeisen, 1967) falls in syenogranite and quartz-rich granitoid fields. b). Tectonic classification using diagram Batchelor and Bowden (1985) shows that all granite samples are in the syn-collision area.

Major Elements

Some results of granite analyses, along with the contained quartz vein samples and some weathering sample analyses, are combined in Table 1 (Toboali) and Table 2 (Air Gegas). These data are used to calculate the Chemical Index of Alteration (CIA). The Chemical Index of Alteration (CIA) approach was applied to determine the weathering ratio of weathered rocks. The number of CIA was calculated in molecular units using the formula: CIA = [Al_2O_3 (Al_2O_3 + CaO + Na_2O + K_2O)] × 100 (%) (Nesbitt and Young, 1982),

Table 1. Major Elements of Weathering Profile Samples from Toboali and the Previous Results of Underlain Granite Samples MN/02B/R, KP/14/R, and the Nearest Outcrops KP/16/R and KP/07F (in %)

Area	South Bangka Toboali															
Sample No	**MN/02/S (0-3 m)**	**MN/02/S (3-6 m)**	**MN/02/ B/R**	**KP/14/CS (0-0.7 m)**	**KP/14/CS (0.7-1.7 m)**	**KP/14/CS (1.7-5.5 m)**	**KP/14/CS (5.5-6.7 m)**	**KP/14/R**	**KP/16/R**	**KP/17/CS (0-0.2 m)**	**KP/17/CS (0.2-2.7 m)**	**KP/17/CS (2.7-3.2 m)**	**KP/17/CS (3.2-4.2 m)**	**KP/17/CS (4.2-5.2 m)**	**KP/17/CS (>5.2 m)**	**KP/07/F**
SiO_2	15.06	20.71	74.53	69.95	73.11	73.11	73.24	74.57	72.4	76.67	78.77	89.79	86.15	88.89	75.11	76.17
TiO_2	2.29	1.46	0.16	0.18	0.19	0.14	0.11	0.09	0.24	0.26	0.29	0.16	0.22	0.19	0.22	0.12
Al_2O_3	43.84	43.69	13.21	17.87	16.77	17.64	14.83	11.67	13.02	11.61	13	5.75	9	1.31	16.29	12.28
Fe_2O_3	16.68	11.85	2.48	3.06	2.75	3.27	2.58	4.02	3.23	1.6	1.25	1.04	0.74	5.92	0.91	2.22
MnO	<0.01	<0.01	0.02	0.01	0.02	<0.01	0.1	0.18	0.04	0.02	0.01	0.01	0.01	0.02	0.01	0.04
MgO	0.79	0.51	0.23	0.09	0.09	0.07	0.17	0.1	0.44	0.1	0.1	0.07	0.08	0.08	0.08	0.13
CaO	0.08	0.03	0.89	0.03	0.02	0.02	0.02	0.04	1.61	0.04	0.02	0.02	0.06	0.03	0.07	0.75
Na_2O	0.26	0.14	2.16	0.03	0.03	0.02	0.12	1.2	2.65	0.06	0.08	0.02	0.01	0.05	0.04	2.42
K_2O	0.32	1.53	5.24	1.14	0.74	0.42	5.57	6.92	5.26	1.25	1.7	0.69	0.63	1.2	2.42	5.69
P_2O_5	0.056	0.005	0.035	0.022	0.02	0.017	0.21	0.019	0.047	0.038	0.018	0.014	0.016	0.015	0.034	0.026
S	0.056	<0.002	0.005	0.01	0.014	0.01	<0.002	<0.002	0.095	<0.002	0.004	<0.002	<0.002	<0.002	<0.002	0.004
Cr_2O_3	0.03	0.04	0.01	<0.01	<0.01	<0.01	<0.01	<0.01	<0.01	<0.01	<0.01	<0.01	<0.1	<0.1	<0.1	<0.1
Lol	19.58	19.18	1.28	7.11	6.34	7.24	2.92	1.01	0.74	7.9	4.7	1.54	2.9	1.46	4.72	0.56
Total	99.0	99.2	100.3	100.3	99.3	99.2	100.0	96.4	99.8	99.5	99.9	99.1	99.8	99.2	99.8	100.4

Table 2. Major Elements of Weathering Profile Samples from Air Gegas and the Previous Results of Underlain Quartz Vein-Granite Contact Samples MN/05E/R and MN/14/R and MN/14/V (in %)

Area	South Bangka Air Gegas								
Sample No	MN/05/S (0-4 m)	MN/05/S (4-8 m)	MN/05/E/R	MN/14/S (0-1.5 m)	MN/14/S (1.5-2 m)	MN/14/S (2-4 m)	MN/14/S (4-5 m)	MN/14/R	MN/14/V
SiO_2	71.93	70.51	84.79	73.63	77.65	70.73	68.69	74.81	96.73
TiO_2	0.15	0.12	0.07	0.3	0.13	0.17	0.21	0.01	0.01
Al_2O_3	17.64	18.63	7.63	15.55	13.02	18.33	20.55	11.89	1.25
Fe_2O_3	3.53	3.61	3.21	3.34	2.72	2.91	2.7	7.88	1.75
MnO	0.01	0.02	0.09	0.01	0.01	0.02	<0.01	0.09	0.03
MgO	0.06	0.04	0.05	0.06	0.02	0.09	0.09	0.12	<0.01
CaO	0.02	<0.01	0.02	0.03	<0.01	<0.01	<0.01	0.04	0.01
Na_2O	0.06	0.04	0.13	0.06	0.02	0.01	0.04	0.79	0.07
K_2O	0.44	0.64	2.18	0.07	0.11	0.59	0.66	0.06	0.02
P_2O_5	0.029	0.027	0.024	0.031	0.021	0.023	0.03	0.026	0.026
S	0.002	<0.002	0.019	0.011	0.008	0.004	0.005	<0.002	<0.002
Cr_2O_3	<0.01	0.01	0.01	<0.01	<0.01	<0.01	<0.01	<0.01	<0.01
Lol	6.45	6.47	0.85	7.24	5.57	6.37	6.99	0.62	<0.02
Total	100.3	100.1	99.1	100.3	99.3	99.2	100.0	94.4	99.9

where CaO content is in silicates. The CIA values of samples range from 58 % to 99 % in both Toboali and Air Gegas (Table 3). This CIA indicates that the sample has generally undergone slight to high weathering.

Rare Earth Elements

All data on REE resulting from the recent study (Tables 3 and 4) were plotted onto spider diagrams of Chondrite-normalized REE (Anders and Grevesse, 1989) to describe the REE patterns in weathering profile and granite.

In the Chondrite normalized REE plot, LREE is generally enriched and HREE is depleted in the Toboali Pluton and the weathering profile, with negative Eu anomalies (Figure 7), except for MN/02/S (3-6 m) where HREE is enriched with very weak negative Eu anomalies (Figure 7a). The profile of KP/17/CS displays a gentle slope REE pattern with a weak negative anomaly of Eu and positive anomaly of Ce (Figure 7b). Samples of profile MN/14/CS has a similar pattern, but a positive anomaly in Ce (Figure 7c). While MN/14/S (Figure 7d) denotes a very steep negative anomaly of Eu with a weak negative anomaly of Ce in REE pattern. Like MN/05/S, the weathering profile MN/14/S indicates a significant negative Eu anomaly in REE pattern (Figure 7e).

XRD and SEM- EDX

Qualitatively and semiquantitatively, the MN/02/S Toboali weathering profile is composed of gibbsite, quartz, cristobalite, tourmaline, and cassiterite minerals for the upper horizon (0-3 m) (Figure 8a). The lower horizon (3-6 m) consists of predominantly kaolinite (55 %), gibbsite (25 %), and goethite (20 %) (Figure 8b).

Samples from weathering profile of KP/14/CS, Toboali, were determined quantitatively. The upper horizon (0.7-1.7 m) shows dominant quartz (73 %) and moderate kaolinite (20 %) (Figure 9). The middle horizon (1.7-5.5 m) comprises a predominance of quartz (65 %) and kaolinite (29 %) (Figure 10). Whereas the lower horizon (5.5-6.7 m) is composed of illite (12 %), quartz (44 %), microcline (37 %), calcite (1 %), and kaolinite (6 %) (Figure 11). The weathering profile of MN/14/S, Air Gegas, detected quantitatively has abundance in quartz (80 %), slightly kaolinite (15 %), and minor gibbsite (4 %) for the upper horizon (1.5-2 m) (Figure 12a), for the middle horizon (2-4 m) has dominant kaolinite (49 %), quartz (46 %), and illite (6 %) (Figure 12b), for the lower horizon (4-5.5 m) showed a predominance of kaolinite (53 %), quartz (38 %), and illite (8%) (Figure 12c). The weathering profile of MN/05/S Air Gegas, the types of minerals detected qualitatively are of quartz, nacrite, anatase, and gibbsite for the

Table 3. REE Analysis Results of Samples from Weathering Profiles and Granite Samples MN/02B/R, KP/14/R, and the nearest Outcrops KP/16/R And KP/07F from Toboali (in ppm)

Area	**South Bangka Toboali**															
Sample No	**MN/02/S (0-3 m)**	**MN/02/S (3-6 m)**	**MN/02/ B/R**	**KP/14/CS (0-0.7 m)**	**KP/14/CS (0.7-1.7 m)**	**KP/14/CS (1.7-5.5 m)**	**KP/14/CS (5.5-6.7 m)**	**KP/14/R**	**KP/16/F**	**KP/17/CS (0-0.2 m)**	**KP/17/CS (0.2-2.7 m)**	**KP/17/CS (2.7-3.2 m)**	**KP/17/CS (3.2-4.2 m)**	**KP/17/CS (4.2-5.2 m)**	**KP/17/CS (>5.2 m)**	**KP/07/F**
La	63.8	93.8	222	30.2	33.4	28.2	31	28	77.2	34.6	46.9	35.1	93.2	38	121	322
Ce	65.2	73.6	437	158	142	76.7	146	67.8	160	68	79.9	36.4	70.4	59.2	158	266
Pr	11	14.9	54.6	7.78	8.22	6.8	8.09	7.35	17.5	8.02	9.6	6.67	14.7	7.79	24.4	58.6
Nd	29	35.6	220	29.1	30.2	25.3	29.6	27	61.6	28.5	33.9	22.2	52.7	27.2	87.9	204
Sm	4.2	4.2	53.7	6.1	6.3	5.5	6.1	6.8	12.5	5.8	7	4.1	9.2	5.2	17.4	45.2
Eu	0.3	1	2.8	0.2	0.3	0.2	0.1	0.3	0.7	0.4	0.6	0.3	0.8	0.4	1.3	2.2
LREE	174.1	233.1	990.1	231.38	220.42	142.7	220.89	137.25	329.5	145.32	177.9	104.77	241	137.79	410	898
Gd	4.3	3.5	51.3	5.4	4.7	4.1	4.3	5.6	10.4	4.4	5.4	3.4	7.8	4.3	14.4	39.3
Tb	0.59	2.9	7.65	0.87	0.72	0.61	0.55	0.93	1.79	0.74	0.81	0.54	1.17	0.64	2.32	5.92
Dy	3.5	2.9	39	5.3	4.3	3.3	2.5	4.6	10.4	4.1	4.9	2.9	6.6	3.5	12.9	32.9
Ho	0.7	0.6	6.3	1	0.8	0.7	0.6	0.8	2.1	0.8	0.9	0.6	1.4	0.7	2.5	5.7
Er	2.6	1.9	15.7	3.8	2.3	1.9	1.2	2.5	6.6	2.4	2.7	1..6	4.4	2	6.9	15.8
Tm	0.4	0.3	2.2	0.6	0.4	0.3	0.2	0.4	1	0.4	0.4	0.2	0.6	0.3	1	2.1
Yb	2.8	1.9	12.7	3.2	2.5	2.1	1.3	2.6	6.9	2.5	2.9	1.6	4.1	2	6.6	13.1
Lu	0.46	0.46	1.65	0.52	0.38	0.3	0.21	0.38	1.01	0.38	0.4	0.24	0.62	0.3	0.94	1.87
HREE	15.35	12.14	136.5	20.69	11.8	13.31	10.86	17.81	40.2	15.72	18.41	11.8	26.69	13.76	47.56	116.69
Σ REE	188.46	235.24	1126.6	252.07	232.22	156.01	231.75	155.06	369.7	161.04	196.31	115.85	267.69	151.53	457.56	1014.69
LREE/ HREE	11.34	18.38	7.25	11	19	11	20	7.75	8.20	9.24	9.66	9.46	9.03	10.03	8.62	7.70
CIA %	98	96	63	98.98	98.94	96.78	96.66	61	58	89.58	87.83	87.73	88.73	88.22	99.02	58

Table 4. REE analysis results of samples from weathering profiles and quartz vein-granite contact samples MN/05E/R and MN/14/R and MN/14/V from Air Gegas

Area	South Bangka Air Gegas								
Sample No	MN/05/S (0-4 m)	MN/05/S (4-8 m)	MN/05/E/R	MN/14/S (0-1.5 m)	MN/14/S (1.5-2 m)	MN/14/S (2-4 m)	MN/14/S (4-5 m)	MN/14/R	MN/14/R/V
La	60.6	49	80	37.9	24.5	68.2	84.5	74.5	62.7
Ce	169	206	131	92.4	72	152	257	201	154
Pr	16.6	14	20.4	8.05	5.4	14.4	17.7	15.8	15.2
Nd	54.1	45.1	80.6	28.3	17.5	45	65.1	58.1	50.1
Sm	11.2	9.7	16.7	4.5	3	7.3	10	10.8	8
Eu	<0.1	<0.1	0.2	<0.1	<0.1	0.1	0.1	0.1	<0.1
LREE	311.5	323.8	329.8	171.15	122.4	286.9	434.3	360.3	290
Gd	7.8	6.6	12.2	2.8	1.9	4.1	5.6	6.5	4
Tb	0.97	0.86	1.35	0.35	0.31	0.7	0.72	0.68	0.56
Dy	4.3	4	10.6	2.3	1.8	3.7	3.6	2.7	2
Ho	0.8	0.8	1.2	0.5	0.5	0.8	0.8	0.4	0.3
Er	2.1	2.4	3.6	1.5	1.2	2.5	2.5	0.9	0.9
Tm	0.3	0.4	0.4	0.2	0.2	0.3	0.4	0.2	0.1
Yb	2.3	2.5	3.7	1.6	1.5	2.5	2.2	0.9	0.8
Lu	0.39	0.43	0.49	0.2	0.19	0.35	0.37	0.12	0.11
HREE	18.96	17.99	33.54	9.45	7.6	14.95	16.19	12.4	8.77
Σ REE	330.46	341.79	363.34	180.6	130	301.85	450.49	372.7	298.77
LREE/ HREE	16.43	18.00	9.83	10.11	16.11	19.19	26.83	29.06	33.07
CIA %	96	96	77	98.98	98.94	96.78	96.66	61	58

upper horizon (0-4 m) (Figure 13a), while for the lower horizon (4-8 m) consists of quartz and kaolinite (Figure 13b).

Chemical compound and element contents determined at spots of SEM-EDX mapping are listed in Table 5. Analysis results of the MN/02B/R Toboali weathering profile show significant values in REO (La, Ce, and Nd) of upper and lower weathering profiles. The granite sample from the basement of the profile has significant values only for REO of La and Nd. The REO values of the middle horizon (b) seem more significant than that of the lower horizon (c).

EPMA and BSE Images

The significant compound of REE determined using EPMA in samples MN/02B/R and MN/05E/R was reported to indicate parisite-(Ce), monazite -(Ce), xenotime-(Y), allanite-(Ce), bastnäsite-(Ce), zircon, thorite, and apatite. Most of these REE minerals are inclusions in rock-forming minerals, predominantly biotite with few plagioclases. Monazite-(Ce) and thorite inclusions and parisite-(Ce) cleavage infilling in biotite were indicated. Whereas a sample of quartz vein-bearing granite (MN/05E/R) Air Gegas depicted parasite-infilling in biotite cleavages, quartz observed as part of a vein in granite contains parisite-(Ce) of fracture in infilling along with a dominant grain of cassiterite. Their chemical composition of EPMA indicated that most REE minerals are present in rock-forming minerals. Among REE minerals are thorite and zircon in biotite, and bastnäsite-(Ce) inclusion in feldspar.

Two supporting samples close to the two main profiles, namely KP-17/CS (5.2 m) in Toboali and MN/14/S (1.5-2 m) in Air Gegas, indicate a weathering product of granite containing REE minerals. BSE images of sample KP-17/CS (5.2 m) of Toboali show apatite and monazite remnants in Figure 14a and Figure 14b, respectively. This suggests that the original monazite-(Ce) crystal seems to have been destroyed by weathering and formed aggregate-like monazite-(Ce). In addition to REE minerals, a euhedral crystal of ilmenite is seen in the fragment (Figure 14c). While BSE images of sample MN/14/S (1.5-2 m), Air Gegas, show a fine grain of monazite-(Ce) in quartz fragment (Figure 14d), anhedral zircon crystal in quartz fragment (Figure 14e), and thorite fills in quartz fragment (Figure 14f). Such fragments reflect a result of a weathering product in which monazite-(Ce) and zircon as resistant REE minerals are still preserved.

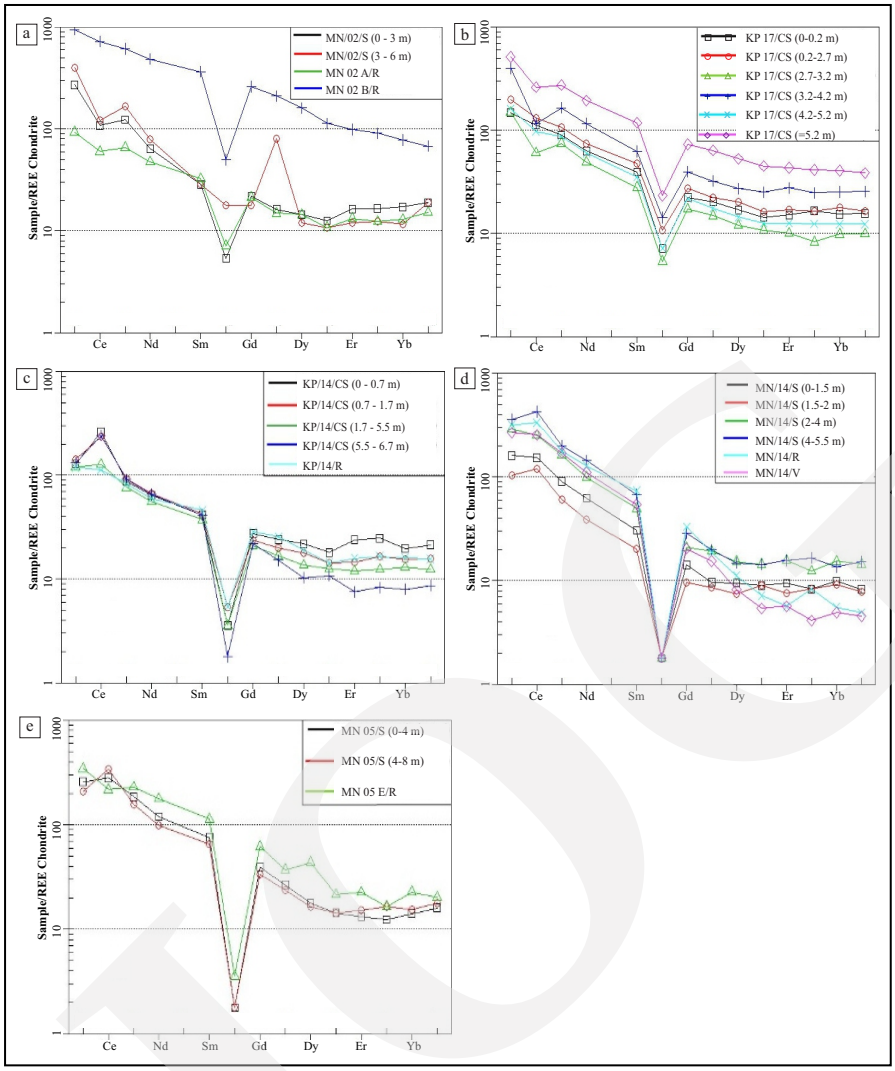

Figure 7. Chondrite normalized-REE patterns of weathering profiles in Toboali: (a) MN/02/S/R, (b) KP/17/CS, (c) KP/14/CS/R, and (d) MN/14/S/R/V; and (e) MN/05/S/R in Air Gegas (Anders and Grevesse, 1989).

Leaching Test

Samples from the horizons of two weathering profiles were selected for the leaching test, namely MN/02/S (3-6 m) Toboali, MN/14/S (2-4 m), and MN/14/S (4-5.5 m) Air Gegas. These zones tend to enrich REE toward lower weathering horizons, coinciding with the dominant component of kaolinite.

The choice of pH 5 is because ion-adsorption clays have hydrated REE ions physisorbed on a negatively charged surface through electrostatic attraction at acidic pH. At pH 9, hydrolyzed and chemisorbed REE on the clay surface through O-REE^{2+} covalent bonds and ion-exchange mechanisms do not release REE into the solution, but in case of presence of REE hydroxides, that are physisorbed on the clays via electrostatic attraction and available for ion exchange at basic conditions (Bradbury and Baeyens, 2002; Feng *et al.*, 2021). REE recovery (R) was calculated using the formula:

$$R = 100 - ((T.t/F.f) \times 100) \quad \text{..... (1)}$$

where:

T is the mass of tailings,

t is tailings assay,

F is the mass of feed, and

f is feed assay (Feng *et al.*, 2021).

The analysis results of ICP-OES for a representative of LREE (La, Ce, and Nd) and HREE

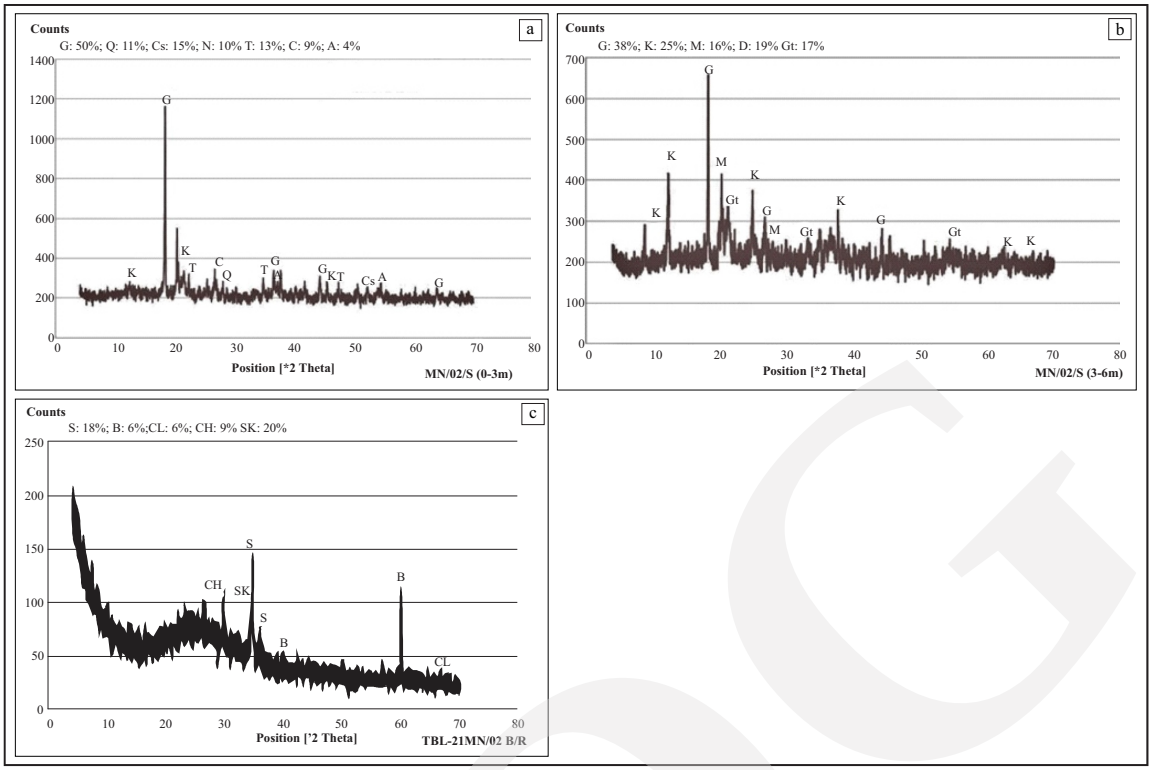

Figure 8. XRD diffractogram of sample (a). MN/02/S (0-3m), (b). MN/02/S (3-6m), and (c). MN/02B/R, Toboali. G = gibbsite, T = tourmaline, Cs = cristobalite, Q = quartz, A = anatase, C = cassiterite, K = kaolinite, M = muscovite, Gt = goethite, S = spinel, B = brucite, CL = calcite, CH = chalcopyrite, and SK = skuterudite.

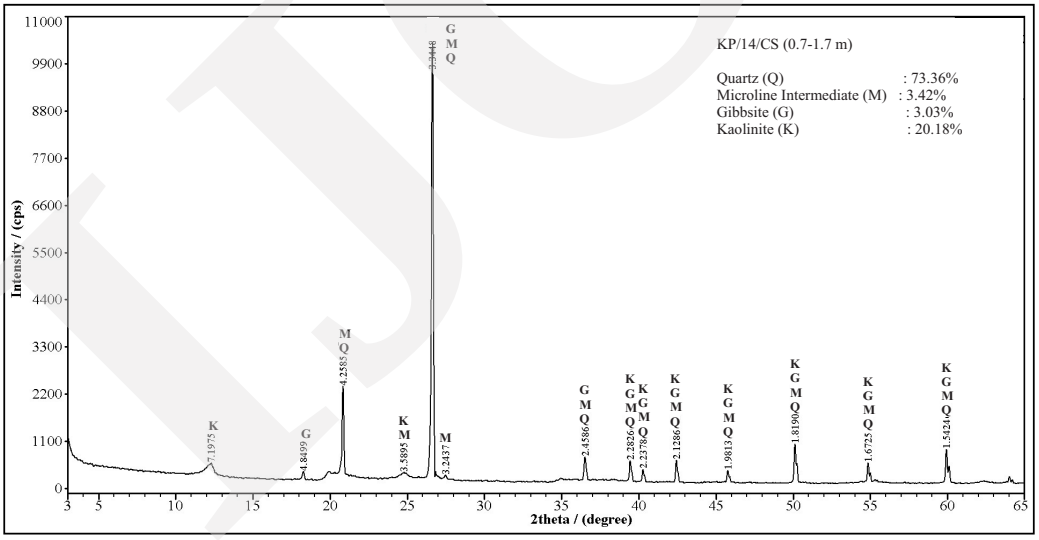

Figure 9. XRD diffractogram of sample KP/14/CS (0.7-1.7 m), Toboali.

(Dy and Y) of tailing or residue are shown in Table 6. Feed assays are referred to the original samples in Tables 3 and 4. The REE recoveries of the leaching test are shown in Table 7.

These results indicate that the La and Ce values of the original sample are lower than the residue samples (tailings) of weathering profile in Toboali. The increased concentration of REE in tailings or residue is suspected due to the two elements being in the hematite mineral phase. Hematite was detected in the XRD diffractogram of sample residue (Figure

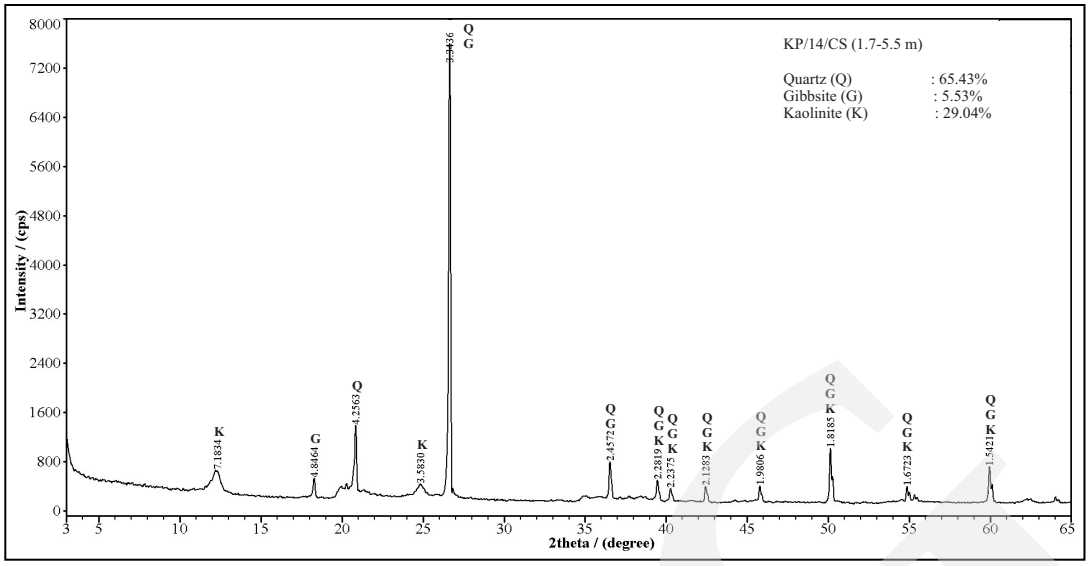

Figure 10. XRD diffractogram of sample KP/14/CS (1.7-5.5 m), Toboali.

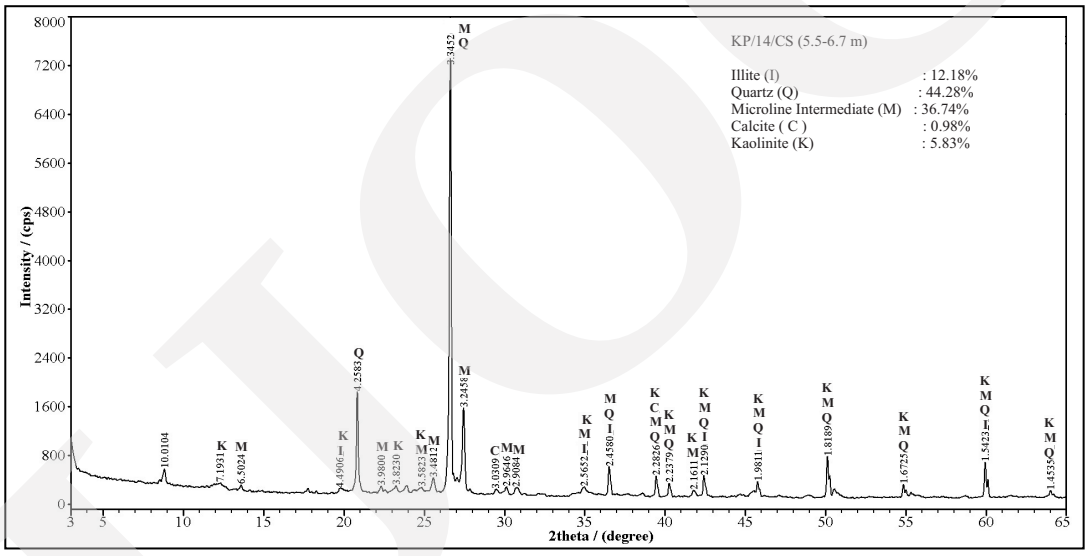

Figure 11. Difractogram of sample KP/14/CS (5.5-6.7 m), Toboali.

15), while goethite was identified in the original sample (Figure 8). This hematite is thought to have resulted from the transformation of REE-bearing goethite by which REE (La and Ce) were not all released but remained in the residue during leaching (Mohapatra *et al.*, 2005). REE extraction with chemically bound iron oxide minerals requires more acidic conditions than simple ion-exchange leaching as in this study (Pangelakis and Moldoveanu, 2014). In contrast, REE in the dissolved ion exchangeable phase was carried in the leachate. Other impurities may have been reduced during leaching, as the consequent REE in the residue is greater than in the original sample.

The leaching test results on two selected weathering profiles (MN/02/S Toboali and MN/14/S Air Gegas) have proven the role of kaolinite as an ion-adsorption clay. The recovery percentage of REEs appears to be higher for HREE (Dy and Y) than LREE. The highest recovery of Ce was achieved in the leaching residue sample MN/14/S (4-5.5 m) Air Gegas. The highest recovery of Nd occurred on this

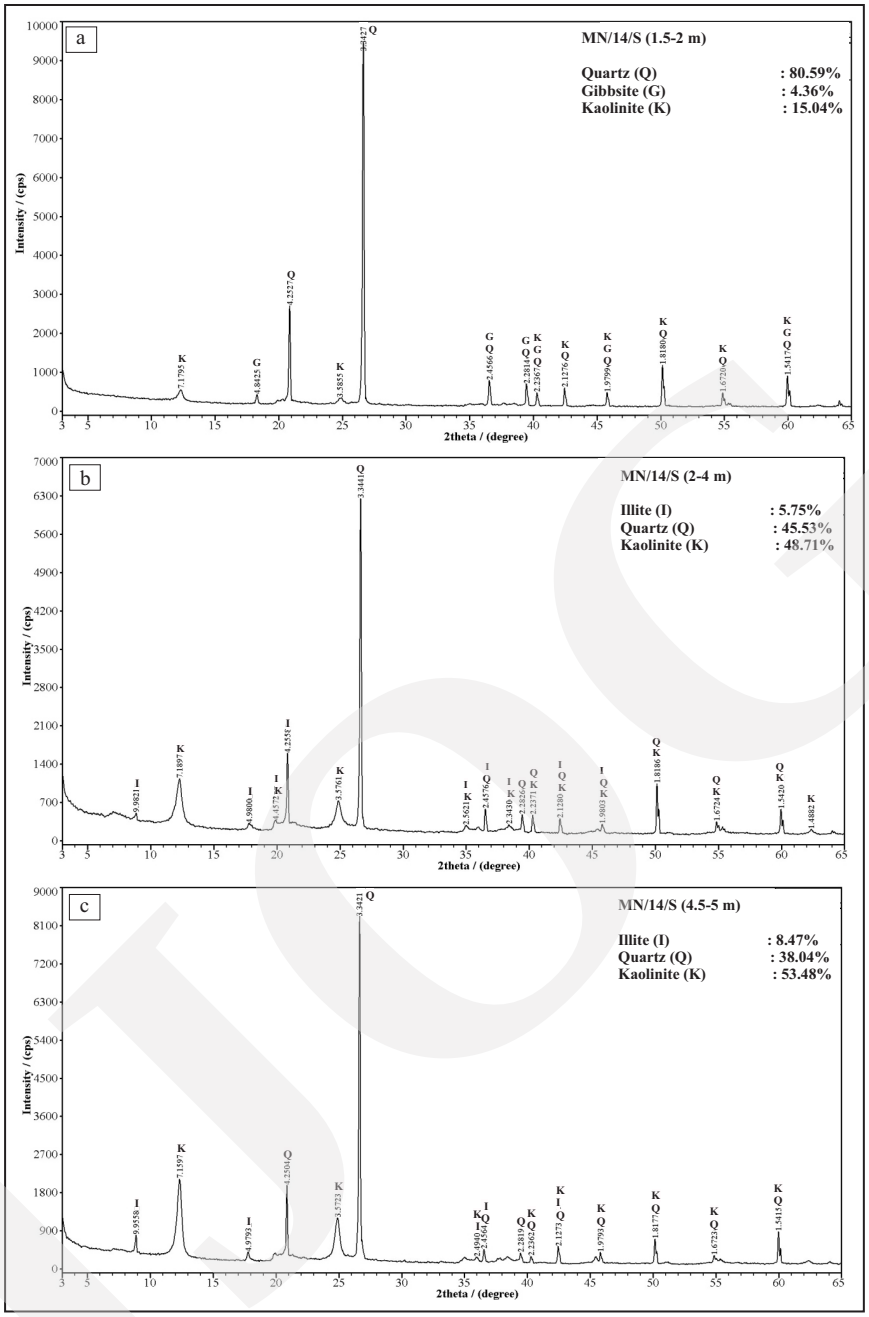

Figure 12. XRD diffractogram of samples (a). MN/14/S (1.5-2m), (b). 21MN/14/S (2-4m), and (c). MN/14/S (4-5.5 m), Air Gegas.

horizon. The percentage recovery of REEs at pH 5 (acid) tends to be higher than at pH 9 (alkaline). The highest recovery was obtained in the C horizon (3-6 m) of weathering profile MN/02/S Toboali at pH 5 (acid), reaching 60 %. However, the recovery of Ce in this layer is low (10 %). LREE recovery, especially La and Ce, is higher on the MN/14/S Air Gegas weathering profile than Toboali (Table 6).

Discussion

REE-Bearing Granite

The LREE/HREE ratio of granite in southern Bangka is enriched in LREE and depleted in HREE, showing moderate to high LREE/HREE ratios within the range of 7.24-12.28. Chondrite-normalized REE patterns of granite samples from Toboali have similarities in

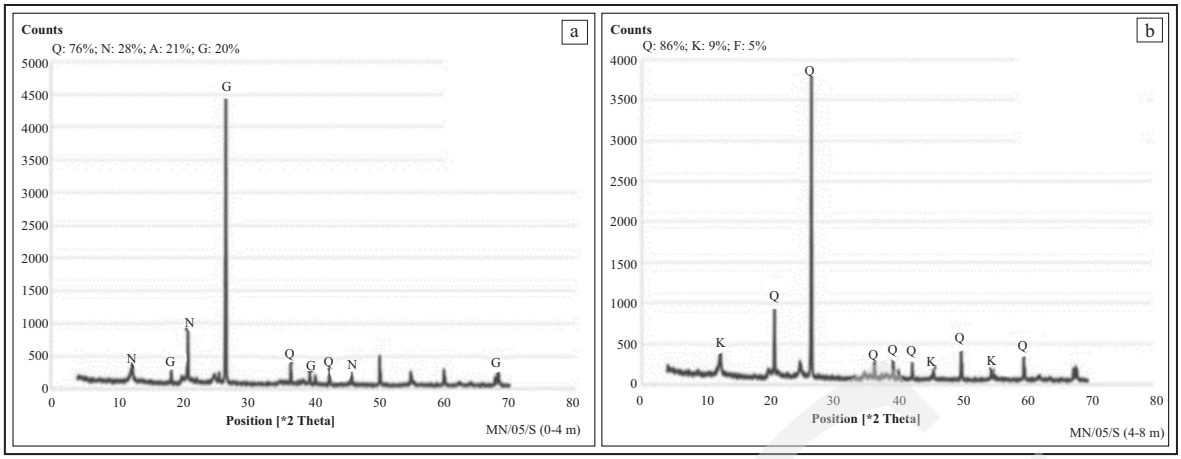

Figure 13. XRD difractogram of sample (a). MN/05/S (0-4m) and (b). MN/05/S (4-8m), Air Gegas. G = gibbsite, N = nacrite, Q = quartz, K = kaolinite, F = Aluminium tetrahydroxodisilicate.

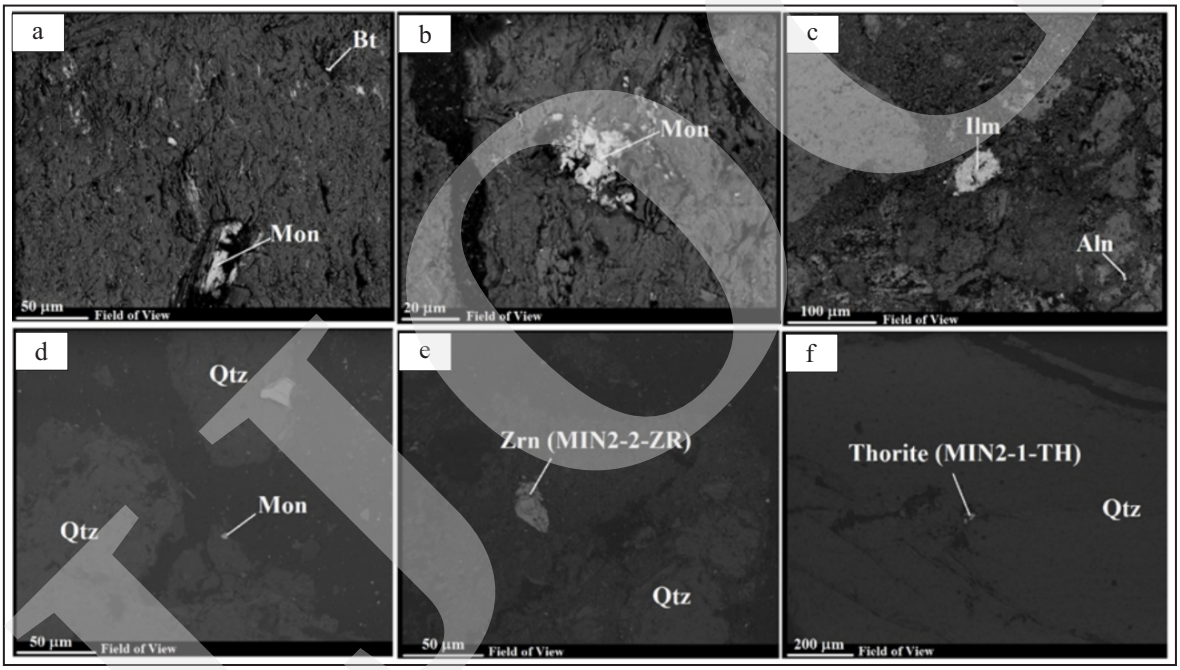

Figure 14. BSE images of sample KP-17/CS (5.2 m) Toboali shows REE bearing-minerals in horizon D with (a). monazite-(Ce) remnant (50 µm) in biotite; and (b). aggregate-like monazite; and (c). fine allanite-(Ce) inclusions (Aln) and a euhedral ilmenite crystal (Ilm). Sample MN/14/S shows the horizon B (1.5-2m) with (d). monazite (Mon) (< 10 µm) in quartz fragment (Qtz); (e). weathered zircon crystal (Zrn) (50 µm) in between quartz fragments of horizon C (2-4 m); (f). thorite (< 10 µm) infill hollows in quartz fragment of horizon D.

REE value trends where enrichment in LREE and depletion in HREE with the negative anomaly of Eu. The normalized REE pattern of one Toboali granite sample, which stands out compared to all samples including the weathering sample, indicates that REE minerals contained were difficult to dissolve. Such REE minerals correspond to REE phosphate, which was resistant to weathering. A slightly negative Eu anomaly in Toboali differs from Gegas Air which has a very sharply negative Eu anomaly. This suggests that the granite of Toboali has undergone weakly differentiated magma to create a poor fractionation of feldspar from magma, unlike in Air Gegas, indicating perfectly fractionated.

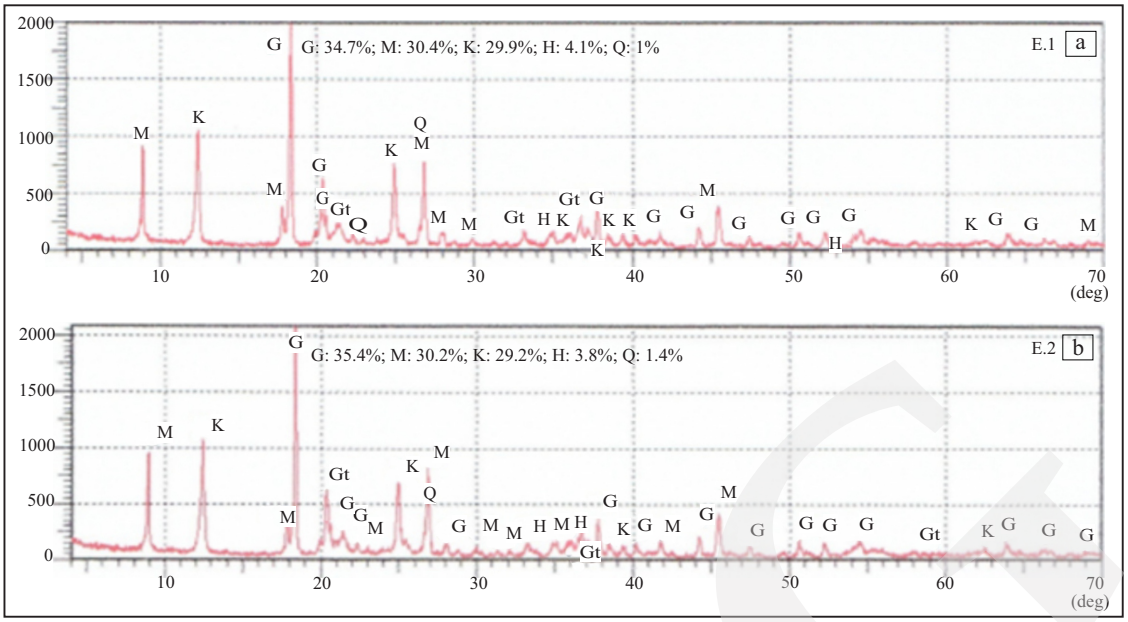

Figure 15. XRD diffractogram of (a). residue MN/02/S (3-6m) at pH = 5, and (b). MN/02/S (3-6m) at pH = 9. G = gibbsite, K = kaolinite, M = muscovite, Q = quartz, H = hematite, deg = 2 theta degree.

Table 5. Compound Analysis of Soil, Rock, and Quartz Vein Samples by SEM-EDX at Selected Spots

	Toboali						Air Gegas			
Sample Number	MN/02/S (0-3 m)		Sample Number	MN/02/S (3-6 m)	Sample Number	MN/02/ B/R	Sample Number	MN/05/S (0-4 m)	Sample Number	MN/05/S (4-8 m)
Wt.% Oxide	SiO_2 24.21		Wt.% Oxide	SiO_2 23.29	Wt.% Oxide	SiO_2 65.75	Wt.% Oxide	SiO_2 46.32	Wt.% Oxide	SiO_2 60.13
	TiO_2 6.18			TiO_2 3.68		ZrO_2 0.37		ThO_2 1.42		Al_2O_3 9.64
	Al_2O_3 40.16			ThO_2 0.52		ThO_2 3.69		Al_2O_3 44.35		Y_2O_3 20.14
	La_2O_3 2.58			Al_2O_3 47.42		Al_2O_3 18.45		La_2O_3 0.22		FeO 6.2
	Ce_2O_3 0.66			La_2O_3 1.35		Ce_2O_3 0.41		Ce_2O_3 0.12		MgO 0.37
	Nd_2O_3 1.1			Ce_2O_3 0.25		Nd_2O_3 0.27		FeO 6.62		K_2O 3.52
	FeO 22.64			Nd_2O_3 0.58		FeO 0.62		MgO 0.95		Total 100
	K_2O 2.47			FeO 20.73		CaO 1.78		Total 100		
	Total 100			K_2O 2.19		Na_2O 3.21				
				Total 100		K_2O 5.45				
						Total 100				

The enrichment of REE is much higher in the granite sample MN/2B/R of Toboali than in other fresh granite in the same location. The suspected monazite-(Ce) inclusions on the thin section were reported to have significant values of Ce, La, and Nd on SEM-EDX mapping (Table 2) that support the REE enrichment in this granite. These REE mineral inclusions are believed to contribute to the elevated REE values up to 1,127 ppm with 990 ppm LREE and 136 ppm HREE. Another high REE value, up to 1,015 ppm, was also detected in sample KP/7/F, not far from MN/02B/R within the same granite pluton in Toboali.

Most REE in granite tends to be concentrated in the form of LREE-rich mineral phases such as apatite, monazite-(Ce)), and fluoro-carbonate minerals and dissolved to enhance LREE enrichment (Xu *et al*., 2017). There are over 250 REE-bearing minerals from which REEs can be extracted. However, 80 % of extracted commercially are obtained from either REE-phosphates (monazite-(Ce) or xenotime-(Y)) or REE fluorocarbonates (bastnäsite-(Ce)) (Han, 2018). This implies that the presence of granite containing a combination of the two REE mineral groups, fluoro-carbonate, and phosphate in the studied

Table 6. Results of the leaching test using 1 M ammonium sulfate solution (raw data in Table 7)

Sample No	MN/02/S (3-6 m)		MN/02/S (3-6 m)		MN/02/S (3-6 m)	MN/14/S (2-4 m)		MN/14/S (2-4 m)		MN/14/S (2-4 m)	MN/14/S (4-5.5 m)		MN/14/S (4-5.5 m)		MN/14/S (4-5.5 m)
	Residue pH : 9 Wi = 5 gr, Wf = 4,25 gr	Recovery (%)	Residue pH : 5 Wi = 5 gr, Wf = 4,24 gr	Recovery (%)	Feed	Residue pH : 5 Wi = 3 gr, Wf = 2.50 gr	Recovery (%)	Residue pH : 9 Wi = 3 gr, Wf = 2.55 gr	Recovery (%)	Feed	Residue pH : 5 Wi = 3 gr, Wf = 2.55 gr	Recovery (%)	Residue pH : 9 Wi = 3 gr, Wf = 2.23 gr	Recovery (%)	Feed
La (mg/kg)	107.64	2	107.64	3	93.8	56.2	31	63.91	20	68.2	66.45	42	68.12	40	84.5
Ce (mg/kg)	77.68	10	75.63	13	73.6	101.12	44	120.08	33	152	179.33	48	182.49	47	257
Nd (mg/kg)	13.98	67	21.61	48	35.6	13.69	75	21.87	59	45	40.26	54	33.84	61	65.1
Dy (mg/kg)	0.78	77	0.8	77	2.9	1.7	62	1.13	74	3.7	1.29	73	1.44	70	3.6
Y (mg/kg)	5.02	70	9.25	45	14.2	7.86	58	8.26	55	15.7	7.22	66	1.44	60	15.8

Table 7. ICP-OES Analysis Results of Residue

Sample No	MN/02/S (3-6 m) pH: 5	MN/02/S (3-6 m) pH: 9	MN/14/S (2-4 m) pH 5	MN/14/S (2-4 m) pH: 9	MN/14/S (4-5.5 m) pH: 5	MN/14/S (4-5.5 m) pH: 9
Ce (mg/kg)	75.63	77.68	101.12	120.08	179.33	182.49
Eu (mg/kg)	1.04	0.97	<0.010	<0.010	<0.010	<0.010
Gd (mg/kg)	3.77	3.14	1.56	2.17	3.42	3.53
La (mg/kg)	107.64	107.64	56.2	63.91	66.45	68.12
Nd (mg/kg)	21.61	13.98	13.69	21.87	40.26	33.84
Pr (mg/kg)	27.1	28.44	15.19	17.2	21.79	22.58
Sc (mg/kg)	16.76	16.55	5.22	5.77	6.56	6.62
Sm (mg/kg)	8.89	8.91	5.56	7.54	9.63	10.12
Dy (mg/kg)	0.8	0.78	1.7	1.13	1.29	1.44
Tb (mg/kg)	10	10.29	3.63	4.68	4.46	4.84
Y (mg/kg)	9.25	5.02	7.86	8.26	7.22	8.57

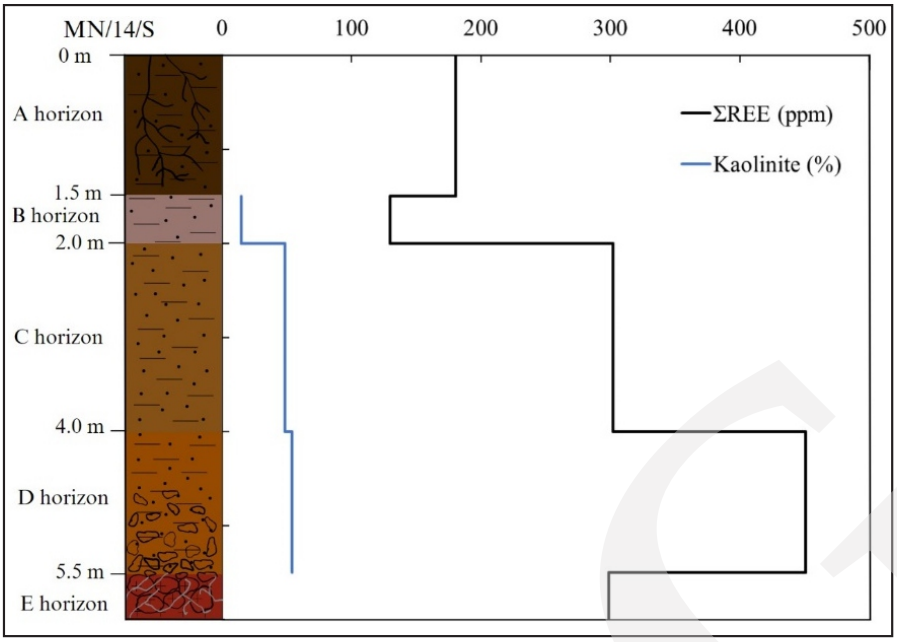

Figure 16. Relationship of ∑REE and kaolinite in the weathering profile of sample MN/14/S, Air Gegas. It appears that both are positively correlated from horizon B to D.

areas can form potential LREE in weathering deposits.

Based on XRD analysis results, no clay as secondary minerals of alteration products were determined in the granite sample of MN/02B/R, Toboali (Figure 8c). Therefore, the higher values in REE of this sample were not connected to REE secondary enrichment. The presence of REE minerals such as monazite-(Ce) and zircon as inclusions in granite is the indicator that possibly formed as primary in the early magmatic stage (Harlov, 2015).

The parent granite under the Toboali and Air Gegas weathering profiles differs in terms of REE content and structure. A whole rock REE assay of samples in Air Gegas (363-373 ppm) (Table 4) is not as much as those in Toboali (367-1127 ppm) (Table 3). This emphasizes the contrasting differences in REE content of both Toboali and Air Gegas underlying weathering profiles. The quartz veins hosted in the granite of the weathering base in Air Gegas represent hydrothermal disturbance. Whether this condition contributes to the low REE on the underlying Air Gegas granite remains to be further investigated.

Enrichment of REE by Weathering

The REE in the weathering profile is sourced from REE-bearing bedrock. The weathering process continues as groundwater moves down, the pH increases as a result of interacting with the rock, and the REEs partition into solid phases, adsorbing onto clay particles or forming secondary REE mineral phases (Verplanck, 2017; Yan *et al*., 2017). The Chemical Index of Alteration (CIA) was calculated to estimate the granite weathering degree. Interval values of CIA refer to the following categories (Nesbitt and Young, 1982): feldspars, including anorthite, albite, and orthoclase, have a CIA value of 50 %. Biotite has CIA values of 65-75 %, and muscovite has a CIA of around 75 %. While clay minerals like illite and kaolinite are common in weathered crust products, CIA values are 75-85 % for illite and 100 % for kaolinite.

Weathering profiles in Toboali (MN/02/S) and Air Gegas (MN/14/S) indicate the enrichment REE in horizon C (Tables 3 and 4). REE enrichment as a late-stage weathering product generally occurs at the lower part of the horizon due to the migration of LREE from the upper part, which joins with the HREE enrichment formed in the

initial stage (Wang *et al*., 2018). The main role of kaolinite as an ion-exchange clay to adsorb dissolved REE is represented by MN/14/S Air Gegas, where the increase in REE value is in line with the rise in the percentage of kaolinite (Figure 16). The REEs are adsorbed through ion exchange and surface complexation on kaolinite under low ionic strength. At high ionic strength, only inner-sphere complexes formed at the surface of kaolinite (Yang *et al*., 2019; Zhao *et al*., 2021). Another research experience indicated that the adsorption of rare earth on kaolin was a spontaneous physisorption process (Xiao *et al*., 2016). Previous studies observed the behaviour of kaolinite as the best absorbent in ion-adsorption deposits compared to other clay groups.

The Air Gegas weathering profile shows REEs enrichment towards depth and the negative Ce anomaly near the surface. This is the characteristic of the ion-adsorption type (Sanematsu *et al*., 2013). The shallow depth is still influenced by relatively acidic surface conditions (low pH). This Ce depletion may occur as a consequence of the oxidation from Ce^{3+} to Ce^{4+} near the surface. In this mechanism, a small amount of Ce^{3+} is transported from the upper part down to the lower part of the profile, leading to REE enrichment (Maulana *et al*., 2014; Yan *et al*., 2017).

The weathering process on REE fluoro-carbonates (parisite-(Ce) and bastnäsite-(Ce)) contained in the basement granite of the profile may have contributed to the enrichment of REE due to the high dissolution rate. While REE phosphates (monazite-(Ce) and xenotime-(Y)) are strongly resistant to weathering and have low solubility (Cetiner *et al*., 2005; Yan *et al*., 2017). Some factors influence the rate of REE-bearing mineral dissolution during weathering granite, including the favourable solubility of REE primary minerals, aqueous complexes, biological activity, groundwater, and clay or secondary minerals (Xu *et al*., 2017).

As REE phosphate is resistant to weathering, some persist in weathering materials such as monazite remnants (Figure 14b), aggregate-like monazite (Figure 14c), and monazite grains (Figure 14a). The lack of REE fluoro-carbonate remnants observed in the BSE images indicates that most were possibly dissolved. Furthermore, groundwater sinking to the bottom of tin pits, the wide distribution of humus in the studied areas, the identified clay minerals, and primary REE minerals are among the factors that played a role in the rate of REE dissolution and their redistribution.

However, it is possible that nano-sized monazite particles formed in the weathering profile horizon other than the fine micron in Air Gegas (Figure 14d) could enrich the REE of the weathering horizon. Precipitation of monazite nanoparticles may form as a result of the release of REE from dissolving rock in an aqueous environment into pore water, which becomes saturated due to the precipitation of clay minerals in the presence of P in solution (Berti *et al*. 2022). This possibility could have happened to the kaolinite weathering profiles at Toboali (Figures 2a and b) and Air Gegas (Figures 2c and d). Proving the existence of these monazite nanoparticles requires TEM (Transmission Electron Microscope) analysis.

Conclusions

The secondary enrichment of REE in the lower horizon of weathering profiles (horizon C) originated from dissolved REE fluoro-carbonate and phosphate minerals contained in the parental granite during the weathering process. With an ion-adsorption mechanism proved using a leaching test indicated kaolinite plays a prominent role as ion-exchangeable clay in absorbing REE cations and precipitating in the Air Gegas weathering horizons. There are also negative Ce anomaly indications on the surface and REE enrichment towards depth as a characteristic of the ion-adsorption type. However, due to the recovery percentage in the leaching test was not maximum, ion-adsorption kaolinite does not provide the only mechanism that accounted for REE enrichment in weathering profile. The possibility of the formation of monazite nanoparticles

deposited with clay mineral causing REE enrichment in the weathering horizon needs further investigation.

Substantial laterites and deposits contained iron oxide, and REE was potentially bound to Fe oxide. However, the restricted REE fluorocarbonate minerals in the parent granite appear to lead to lower REE enrichment in the weathering profile. While the REE phosphate minerals are mostly resistant, they remain in the profile or are mobilized into accumulations of alluvial deposits.

Acknowledgments

The authors express great acknowledge to the Director-General of Mineral and Coal of Indonesia for funding the REE inventory project 2021, the Head of Centre for Mining Technology Development, and the Head of the Centre for Mineral Coal and Geothermal Resources for appointing Armin Tampubolon as the team coordinator and for allowing him to use the data for this project.

References

Alshameri, A., Wang, X.W.H., Fuguo, Y., Chen, X., He, H., Yan, C., and Xu, F., 2019. A Review of the Role of Natural Clay Minerals as Effective Adsorbents and an Alternative Source of Minerals. *In:* Essa, K.S. (ed.), *Minerals*, p.49-64. DOI: 10.5772/intechopen.87260.

Anders, E. and Grevesse, N., 1989. The Abundances of the Elements: *Meteoritic and Solar. Geochimica et Cosmochimica Acta,* 53, p.197-214. DOI: 10.1016/0016-7037(89)90286-X.

Aryanto, N.C.N. and Kamiludin, U., 2016. The Content of Placer Heavy Mineral and Characteristics of REE at Toboali Coast and Its Surrounding Area Bangka-Belitung Province. *Bulletin of the Marine Geology,* 31 (1), p.45 -54. DOI: 10.32693/bomg.31.1.2016.318.

Aryanto, N.C.N. and Kamiludin, U., 2016. The Content of Placer Heavy Mineral and Characteristics of REE at Toboali Coast and Its Surrounding Area Bangka-Belitung Province. *Bulletin of the Marine Geology,* 31 (1), p.45-54.

Batchelor, R.A. and Bowden, P., 1985. Petrogenetic Interpretation of Granitoid Rock Series Using Multicationic Parameters. *Chemical Geology,* 48, p.43-55. DOI: 10.1016/0009-2541(85)90034-8

Berti, D., Slowey, N.C., Yancey, T.E., and Deng, Y., 2022. Rare earth nano minerals in bentonite deposits of the Eocene Texas coastal plains. *Applied Clay Science,* 216,106373. DOI: 10.1016/j.clay.2021.106373.

Borst A.M., Smith, M.P., Finch, A.A., Estrade, G., Benavent, C.V., Nason, P., Marquis E., Horsburgh N.J., Goodenough, K.M., Xu X., Kynicky, J., and Geraki, K., 2020. Adsorption of rare earth elements in regolith-hosted clay deposits. *Nature Communications*, 11, 4386. DOI: 10.1038/s41467-020-17801-5.

Bradbury, M.H. and Baeyens., B., 2002. Sorption of Eu on Na- and Ca-montmorillonites: experimental investigations and modeling with cation exchange and surface complexation. *Geochimica et Cosmochimica Acta,* 66, p.2325-2334. DOI: 10.1016/S0016-7037(02)00841-4.

Cetiner, Z.S., Wood, S.A., and Gammons, C.H., 2005. The aqueous geochemistry of the rare earth elements, Part XIV. The solubility of rare earth element phosphates from 23 to 150 C. *Chemical Geology,* 217, p.147-169. DOI: 10.1016/j.chemgeo.2005.01.001

Chung, F.H., 1974. Quantitative interpretation of X-ray diffraction patterns of mixtures. II. Adiabatic principle of X-ray diffraction analysis of mixtures. *Journal of Applied Crystallograph,* 7, p.526-531. DOI: 10.1107/S0021889874010387

Coppin, F., Berger, G., Bauer, A., Castet, S., and Loubet, M., 2002. Sorption of lanthanides on smectite and kaolinite. *Chemical Geology,* 182, p.57-68. DOI: 10.1016/S0009-2541(01)00283-2

Crow, M.J. and Van Leeuwen, T.M. 2005. Metallic mineral deposits. Geological Society,

London, *Memoirs,* 31, p.147-174. DOI: 10.1144/gsl.mem.2005.031.01.12

Dickson, J.S., 2015. Rare earth elements: Global market overview. Symposium on critical and strategic materials. *British Columbia Geological Survey Paper,* 3, p.5-11.

Feng, X., Onel, O., Troche, M.C., Noble, A., Yoon, R.H., and Morris, J.R., 2021. Study of rare earth ion-adsorption clays: the speciation of rare earth elements on kaolinite at basic pH, *Applied Clay Science,* 201, 105920. DOI: 10.1016/j.clay.2020.105920.

George, J.S., Carlee, A., and Suzanne, P. 2015. Which materials are 'critical' and 'strategic'. Symposium on critical and strategic materials. *British Columbia Geological Survey Paper,* 3, p.1-6.

Hamdan, Z.A. and Rusmana, E., 2003. The origin of iron oxide within weathered granite and alluvial tin deposition South Bangka District, Bangka Belitung. *Majalah Geologi Indonesia,* XVIII (2), p.95-105.

Hamdan, Z.A. 2004. An NW-SE trending zone of primary tin mineralization in North Bangka, Indonesia: Geology Distribution and Origin. *Majalah Geologi Indonesia,* 19 (3), p.173-185.

Han, K.N., 2018. Effect of Anions on the Solubility of Rare Earth Element-Bearing Minerals in Acids. *Mining, Metallurgy and Exploration,* 36 (3), p.215-225. DOI: 10.1007/s42461-018-0029-3.

Harlov, D.E. 2015. Apatite: A fingerprint for metasomatic processes. *Elements,* 11 (3), p.171-176. DOI: 10.2113/gselements.11.3.171.

Imai, A., 2009. *Rare Earth Elements in Weathered Crusts of Granitic Rocks in Southeast Asian Tin Belt (Northern Thailand, Southern Thailand (Ranong-Takua Pa-Phuket) and Bangka Island, Indonesia).* Repository UGM.

Irzon, R., Syafri, I., Hutabarat, J. and Sendjaja, P., 2016. REE Comparison Between Muncung Granite Samples and their Weathering Products, Lingga Regency, Riau Islands. *Indonesian Journal on Geoscience,* 3 (3), p.149-161. DOI: 10.17014/ijog.3.3.149-161

Kurnia, S.W. and Priadi, B., 2013. Petrography and Geochemical Major Elements of Granite in Bangka Island: Initial Evaluation of Tectonomagmatisme. *Eksplorium,* 34 (2), p.1-16 (in Indonesian).

Li, Y.H.M., Zhao, W.W. and Zhou, M.F., 2017. Nature of parent rocks, mineralization styles and ore genesis of regolith-hosted REE deposits in South China: an integrated genetic model. *Journal of Asian Earth Sciences,* 148, p.65-95. DOI: 10.1016/j.jseaes.2017.08.004

Mangga, S.A. and Djamal, B., 1994. Geologic *Map of North Bangka Quadrangle, Scale 1: 250,000.* Geological Development and Research Center, Bandung, Indonesia.

Margono, U., Supandjono, E. and Partoyo, E., 1995. *Geologic Map of South Bangka Quadrangle, Scale 1: 250,000.* Geological Development and Research Center, Bandung, Indonesia.

Marker, H.J.D., 2013. Distinction of Magma Genesis between The Tin Bearing Granitoid Rocks of The Indonesian Tin Belt Islands and the Tin Barren Granitoid Rocks. *Jurnal Sumber Daya Geologi,* 23 (2) (in Indonesian).

Maulana, A., Yonezu, K., and Watanabe, K., 2014. Geochemistry of rare earth elements (REE) in the weathered crusts from the granitic rocks in Sulawesi Island, Indonesia. *Journal of Earth Sciences,* 25 (3), p.460-472. DOI: 10.1007/s12583-014-0449-z.

McDonough, W.F. and Sun, S.S., 1989. Chemical and isotopic systematics of oceanic basalts: Implications for mantle composition and processes. *Geological Society London Special Publications*, 42, p.313-345. DOI: 10.1144/GSL.SP.1989.042.01.19

Mohapatra, M., Sahoo, S. K., Mohanty, C. K., Das, R. P., and Anand, S., 2005. Effect of Ce(IV) doping on formation of goethite and its transformation to hematite. *Materials Chemistry and Physics,* 94 (2-3), p.417-422. DOI:10.1016/j.matchemphys.2005.05.024.

Moldoveanu, G.A. and Papangelakis, V.G., 2016. An overview of rare-earth recovery by ion-exchange leaching from ion-adsorption

clays of various origins. *Mineralogical Magazine,* 80 (1), p.63-76. DOI: 10.1180/minmag.2016.080.051.

Nesbitt, H.W. and Young. G.M., 1982. Early Proterozoic Climates and Plate Motions Inferred From Major Element Chemistry of Lutites, *Nature,* 299, p.715-717.

Ng. S.W.P., Martin J.W., Muhammad H.R., Claudia, T., Sayed, M., Grahame J.H.O., Azman A.G. and Su-Chin, C., 2017. LateTriassic granites from Bangka, Indonesia: A continuation of the Main Range granite province of the South-East Asian Tin Belt. *Journal of Asian Earth Sciences,* 138, p.548-561.

Pangelakis, V.G. and Moldoveanu, G., 2014. Recovery of Rare Earth Elements from clay minerals. *ERES2014: 1st European Rare Earth Resources Conference|Milos|04-07/09/2014.*

Phillip, L.V., 2017. The role of fluids in the formation of rare earth element deposits, *Procedia Earth and Planetary Science,* 17, p.758-761.

Sanematsu, K., Yasushi, W., Murakami, H., Sixomxenn, D.S., and Siphandone, V., 2009. Enrichment of REE in granitic rocks and their weathered crusts in Central and Southern Laos. *Bulletin of the Geological Survey of Japan,* 60, p.527-558.

Sanematsu, K., Kon, Y., Imai, A., Watanabe, K. and Watanabe, Y., 2013. Geochemical and mineralogical characteristics of ion-adsorption type REE mineralization in Phuket, Thailand. *Minerlium Deposita,* 48, p.437-451. DOI 10.1007/s00126-011-0380-5.

Schwartz, M.O., Rajah, S.S., Askury, A.K., Putthapiban, P. and Djaswadi, S., 1995. The Southeast Asian Tin Belt. *Earth-Science Reviews,* 38 (2-4), p.95-293. DOI: 10.1016/0012-8252(95)00004-T

Shita, K. and Lucas, D.S., 2009. *Characteristics of granitic rocks of Bangka Island, Indonesia, and their associated mineralization (Master thesis).* Yogyakarta: Gajah Mada University of Geological.

Streckeisen, A., 1967. Classification and nomenclature of igneous rocks. *Nues Jahrbuch fur mineralogie Abhandlungen,* 107, p.144-420.

Terry, R.D. and Chilingar, G.,V., 1955. Summary of "concerning some additional aids in studying sedimentary formations" by M.S. Shvetsov. *Journal of Sedimentary Petrology,* 25 (3), p.225-234. DOI: 10.1306/74d70466-2b21-11d7-8648000102c1865d

Verplanck, P.L., 2017. The role of fluids in the formation of rare earth element deposits. *Procedia Earth and Planetary Science,* 17, p.758-761. DOI: 10.1016/j.proeps.2017.01.014.

Wang, D., Zhi Zhao, Z., Yua, Y., Daia, J., Deng, M., Zhaoa, T. and Liua, L., 2018. Exploration and research progress on ion-adsorption type REE deposit in South China. *China Geology,* 3, p.415-442. DOI: 10.31035/cg2018022.

Weng, Z.H., Gavin, M.M., Simon, M.J. and Nawshad, H., 2017. *A*ssessment of Global Rare Earth Supply and Wind Energy Growth: Opportunities and Challenges. *Green and Sustainable Chemistry Conference, Berlin, Germany.* 4-17th May. 2017.

Wu, C., Huang, D., and Guo, Z., 1990. REE Geochemistry in the Weathered Crust of Granites, Longnan Area, Jiangxi Province. *Acta Geologica Sinica,* 3 (2)*, p.*193-209. DOI: 10.1111/j.1755-6724.1990.mp3002006.x

Xiao *et al*., 2016? p.14

Xu, C., Kynický J.,P., Smith, M.P., Kopriva, A., Brtnický, M., Urubek, T., Yang, Y., Zhao, Z., He, C., and Song, W., 2017. Origin of heavy rare earth mineralization in South China. *Nature Communication,* 8, 14598p. DOI: 10.1038/ncomms14598.

Yan, H.M., Li, W., Winston, Zhao, M., and Zhou, F., 2017. Nature of parent rocks, mineralization styles and ore genesis of regolith-hosted REE deposits in South China: An integrated genetic model. *Journal of Asian Earth Sciences,* 148, p.65-95. DOI: 10.1016/j.jseaes.2017.08.004

Yang, M., Xiaoliang, Liang, X., Ma, L., Jian Huang J., He, H., Jianxi, and Zhu, J., 2019. Adsorption of REEs on kaolinite and halloysite: A link to the REE distribution on clays in the weathering crust of granite. *Chemical Geology,* 525, p.210-219. DOI: 10.1016/j.chemgeo.2019.07.024

Zhang, S., Liu, Q., Gao, F., Li, X., Liu, C., Li, H., Boyd, S.A., Johnston, C.T., and Teppen, B.J., 2017. Mechanism Associated with Kaolinite Intercalation with Urea: Combination of Infrared Spectroscopy and Molecular Dynamics Simulation Studies. *The Journal of Physical Chemistry C,* 121 (1), p.402-409. DOI: 10.1021/acs.jpcc.6b10533

Zhao, J., Wang, Z., Gao, W., Wang, Y.F., and Huang, B.W., 2021. Theoretical Investigation on Rare Earth Elements of Y, Nd, and La Atoms' Adsorption on the Kaolinite (001) and (001) Surfaces, *Minerals,* 11 (8), 00856. DOI: 10.3390/min1108085.Batus; es hilinatus op